ISTANBUL TECHNICAL UNIVERSITY ★ GRADUATE SCHOOL

QUANTIFYING UNCERTAINTIES IN NUMERICAL PREDICTIONS OF DYNAMIC CAVITATION

M.Sc. THESIS

Erdinç KARA

Department of Shipbuilding and Ocean Engineering

Shipbuilding and Ocean Engineering Programme

JUNE 2023

ISTANBUL TECHNICAL UNIVERSITY ★ GRADUATE SCHOOL

QUANTIFYING UNCERTAINTIES IN NUMERICAL PREDICTIONS OF DYNAMIC CAVITATION

M.Sc. THESIS

Erdinç KARA
(508201107)

Department of Shipbuilding and Ocean Engineering

Shipbuilding and Ocean Engineering Programme

Thesis Advisor: Prof. Dr. Ömer Kemal KINACI
Thesis Co-Advisor: Dr. Artur K. LIDTKE

JUNE 2023

İSTANBUL TEKNİK ÜNİVERSİTESİ ★ LİSANSÜSTÜ EĞİTİM ENSTİTÜSÜ

DİNAMİK KAVİTASYONUN SAYISAL TAHMİNLERİNDEKİ BELİRSİZLİKLERİN ÖLÇÜMÜ

YÜKSEK LİSANS TEZİ

Erdinç KARA
(508201107)

Gemi ve Deniz Teknolojisi Mühendisliği Anabilim Dalı

Gemi ve Deniz Teknolojisi Mühendisliği

Tez Danışmanı: Prof. Dr. Ömer Kemal KINACI
Tez Eş-Danışmanı: Dr. Artur K. LIDTKE

HAZİRAN 2023

Erdinç KARA, a M.Sc. student of ITU Graduate School student ID 508201107 successfully defended the thesis entitled " QUANTIFYING UNCERTAINTIES IN NUMERICAL PREDICTIONS OF DYNAMIC CAVITATION", which he prepared after fulfilling the requirements specified in the associated legislations, before the jury whose signatures are below.

Thesis Advisor :	**Prof. Dr. Ömer Kemal KINACI** Istanbul Technical University
Co-advisor :	**Dr. Artur K. LIDTKE** Maritime Research Institute Netherlands
Jury Members :	**Prof. Dr. Ömer GÖREN** Istanbul Technical University
	Doç. Dr. Uğur Oral ÜNAL Istanbul Technical University
	Dr. Bülent DÜZ Maritime Research Institute Netherlands

Date of Submission : **15 May 2023**
Date of Defense : **15 June 2023**

To my precious sister, Gülden..

FOREWORD

I would like to thank my esteemed advisors, Prof. Dr. Ömer Kemal KINACI and Dr. Artur K. LIDTKE, who meticulously directed this study, did not spare any kind of encouragement and sacrifice, and whose support I felt at all times, the Maritime Research Institute Netherlands (MARIN) for providing me an intership opportunity and great facilities and my supervisors in there Dr. Bülent DÜZ and Douwe RIJPKEMA for sharing their knowledge with me and patiently guiding me.

I would also like to thank the Türk Loydu Foundation for providing me with scholarship throughout my graduate education.

Besides, I would like to thank Res. Asst. Feride KUTBAY for her helps in many ways and, my dear girlfriend İlayda ŞAHİN, my close friends Hıdırcan CUZDAN, Mehmet Akif TARHAN, Derya ÇELİKEL and Sude ÇELİKEL who are always there for me.

I would like to express my deepest gratitude to my whole family, especially my sister Gülden ACIL, who brought me to where I am today, provided all kinds of opportunities with unlimited devotion, and whose love, attention and support I always felt.

JUNE 2023

Erdinç KARA
(Research Assistant)

TABLE OF CONTENTS

ABBREVIATIONS

AHF	**:** Adaptive Hybrid Functions
ANN	**:** Artificial Neural Network
AoA	**:** Angle of Attack
CDF	**:** Cumulative Distribution Function,
CFD	**:** Computational Fluid Dynamics
CI	**:** Confidence Interval
DES	**:** Detached Eddy Simulation
DoE	**:** Design of Experiments
DR	**:** Dimension Reduction
ECDF	**:** Empirical Cumulative Distribution Function
EDF	**:** Empirical Cumulative Distribution Function
FFNI	**:** Full Factorial Numerical Integration
FORM	**:** First-Order Reliability Method
HSS	**:** Hammersley Sequence Sampling
KCD	**:** King's College Doha
KLE	**:** Karhunen–Loeve Expansions
KSKL	**:** Scale-Adaptive-Simulation Model
LHS	**:** Latin Hybercube Sampling
MARIN	**:** Maritime Research Institute Netherlands
MARS	**:** Multivariate Adaptive Regression Splines
MCS	**:** Monte Carlo Simulation
MIT	**:** Massachusetts Institute of Technology
MLS	**:** Moving Least Squares
MPP	**:** Most Probable Point
PCE	**:** Polynomial Chaos Expansion
PHV	**:** Propeller Hull Vortex
RANS	**:** Reynolds-Averaged Navier-Stokes
RBF	**:** Radial Basis Function
SALib	**:** Sensitivity Analysis Library
SCAT	**:** Samsung Cavitation Tunnel
SORM	**:** Second-Order Reliability Method
UP	**:** Uncertainty Propagation
UQ	**:** Uncertainty Quantification
URANS	**:** Unstable Reynolds-Averaged Navier-Stokes
URN	**:** Underwater Radiated Noise

SYMBOLS

α	: Angle of attack
α_v	: Vapor volume fraction
P_0	: Atmospheric Pressure
P_v	: Vapor Pressure
σ	: Cavitation number
σ_0	: Free-stream cavitation number
$\sigma_{0.7}$	: Cavitation number at 0.7R of propeller blade
ρ	: Density
ρ_w	: Water Density
ρ_v	: Vapor Density
C_L	: Lift Coefficient
C_D	: Drag Coefficient
c	: Chord lenght
s	: Span lenght
Re	: Reynolds number
D	: Propeller diameter
A_E	: Expanded area of the propeller blade
A_P	: Projected area of the propeller blade
$\mathbf{J}$	: Advance coefficient
V_A	: Advance Velocity
τ_c	: Thrust load coefficient
T	: Thrust Produced by the Propeller
n	: Propeller rotation rate (rps)
ν_B	: Vapor kinematic viscosity
L_{cav}	: Cavitation lenght
V_{cav}	: Cavitation volume
χ_{grid}	: Discretization uncertainty
μ	: Dynamic viscosity
U_∞	: Inflow velocity
S_i	: Sobol indices
ST_i	: Total-order Sobol indices

LIST OF TABLES

Page

LIST OF FIGURES

Page

QUANTIFYING UNCERTAINTIES IN NUMERICAL PREDICTIONS OF DYNAMIC CAVITATION

SUMMARY

In engineering and physics applications, cavitation is a physical phenomenon can be encountered in various fluid systems including pumps, turbines, and propellers, when the pressure of the fluid drops below the vapor pressure, and causes the fluid to evaporate and form small bubbles or voids in the fluid. Cavitation in marine propellers is a critical issue due to its adverse effects on many aspects of operations such as causing noise and vibration, damaging the propeller structural integrity and reducing propulsion efficiency. Therefore, accurate estimation of cavitation from the early stages of design is important to provide better propeller design. However, numerically predicting the cavitation behavior is a difficult task due to the complexity of the problems, the high computational cost of simulations, and various numerical uncertainties. Considering the numerical methods used in the determination of propeller cavitation, it is seen that the use of computational fluid dynamics (CFD) has increased simultaneously with the rapidly advancing computer technology. However, there are various uncertainties that can have important effects on the results such as the input parameters used in the simulations, the quality of the network, the physics models used, the modeling of the computational space, and the definition of the boundary and initial conditions. In the literature, there are various studies in many different areas related to uncertainty quantification and sensitivity analysis. Simultaneously with the increase in the use of CFD tools, studies on the application of uncertainty quantification approaches to CFD problems are gaining momentum. Although there are many studies on numerical analysis of cavitation or uncertainty analysis studies applied on CFD problems in the literature, no studies were found in which numerical uncertainty analysis was performed on the cavitation phenomenon. For this reason, in the current thesis study, the analysis of input parameters and discretization uncertainties separately and together in the numerical estimation of cavitation is emphasized. Since three-dimensional numerical simulation of propeller cavitation is espensive in computational cost, in this study, cavitation behavior on a two-dimensional hydrofoil was investigated as a test case to estimate parameter and discretization uncertainties and combine them into a single value. The test case is selecected as the NACA 66 foil, which has been experimentally studied by many researchers before. Angle of attack and cavitation number were chosen as input parameters and their effects on properties such as force coefficients (lift and drag) and cavitation properties were investigated. ReFRESCO, the internal code of the Maritime Research Institute Netherlands (MARIN), was used in all simulations in the study. Sobol indices were calculated to measure the relative importance of the input parameter and discretization uncertainties. In addition, discretization uncertainty is considered as the third input parameter to investigate the effect of discretization uncertainty on output

parameters. Instead of sampling the large number of samples needed for uncertainty quantification analysis, a suitable surface is defined with data generated with only 25 sampling points. Only CFD simulations of these points were performed. Then, using the surrogate model approach from the results obtained, separate response surfaces were created for each of the output parameters; Sobol indices were calculated precisely by taking 2^{15} points from these response surfaces.

The results show that confidence intervals and Sobol indices for input parameters such as drag coefficient (C_D) and cavitation length (L_{cav}) remain mostly unchanged despite changes in grid refinement; shows that parameter uncertainties are the dominant factor for these output parameters. Regarding the lift coefficient (C_L), it was observed that the effect of discretization uncertainty was larger than C_D and V_{cav}, but still parameter uncertainty had a more significant effect than discretization uncertainty. Contrary to other output parameters, the results for the cavitation volume (V_{cav}) parameter show that discretization uncertainty has a greater effect on this parameter than the parameter uncertainty. However, the study still showed that parameter uncertainty plays an important role in determining this output parameter.

For future research, the scope of this study can be expanded to develop a formulation can be that considers the effects of iterative uncertainty or time step uncertainty as well as measuring discretization and input uncertainty for time-unsteady-flow applications. Other parameters, such as coefficients related to turbulence or cavitation models, can be included in the analyzes to account for additional degrees of modeling uncertainties in addition to grid and operating point conditions.

DİNAMİK KAVİTASYONUN SAYISAL TAHMİNLERİNDEKİ BELİRSİZLİKLERİN ÖLÇÜMÜ

ÖZET

Kavitasyon, sıvı akışkanın söz konusu olduğu sistemlerde, sıvının basıncının buhar basıncının altına düştüğünde sıvının buharlaşmasına ve sıvı içinde küçük kabarcıklar veya boşluklar oluşturmasına neden olan fiziksel bir olgudur. Bu kabarcıklar daha sonra, daha yüksek basınçlı bir alana hareket ettiklerinde çöker veya patlayarak yakındaki yapılara veya makinelere zarar verebilecek bir şok dalgasına neden olur. Bu yönü nedeniyle mühendislikte ve fizikte kavitasyon, pompalar, türbinler ve pervaneler dahil olmak üzere çeşitli sıvı sistemlerinde karşılaşılabilen, sistem dizayn aşamasındayken düşünülmesi ve bazı özel durumlar (süperkavitasyon gibi) hariç kaçınılması gereken bir problemdir.

Deniz taşıtlarının pervanelerinde kavitasyon, gürültü ve titreşime neden olması, pervane yapısal bütünlüğünde hasara yol açması ve sevk verimini düşürmesi gibi operasyonların birçok yönü üzerindeki olumsuz etkileri nedeniyle kritik bir konudur. Bu nedenle, daha iyi pervane tasarımı sağlamak için dizaynın erken safhalarından itibaren kavitasyonun doğru tahmini ve minimize edilmesi önemlidir. Ancak, kavitasyon davranışını sayısal olarak tahmin etmek, problemlerin karmaşıklığı, simülasyonların yüksek hesaplama maliyeti ve çeşitli sayısal belirsizlikler nedeniyle zor bir iştir. Pervane kavitasyonunun tayininde kullanılan sayısal yöntemlere bakıldığında, sınır eleman yöntemleri, kaldırıcı hat yöntemleri ve hesaplamalı akışkanlar dinamiği (HAD) simülasyonları görülmektedir. Literatürde söz konusu yöntemler ile ilgili birçok çalışma yer almaktadır. Bilhassa son zamanlarda akışkanlar ile ilgili problemlerin çözümünde hızla ilerleyen bilgisayar teknolojisi ile eş zamanlı olarak HAD yöntemlerinin de kullanımı artmıştır. Bununla birlikte, yapılan simülasyonlarda kullanılan girdi parametreleri, ağ kalitesi, kullanılan fizik modeller, hesaplama alanının modellenmesi, sınır ve başlangıç koşullarının tanımlanması gibi sonuçlar üzerinde önemli etkileri olabilecek çeşitli belirsizlikler söz konusudur.

Belirsizlik kavramı en basit ifade ile 'kesin olarak bilinmeyen şeyler' olarak tanımlanabilir. Bir problemdeki daha fazla belirsizlik, kesinliğin veya güvenilirliğin azalmasına neden olur. Analistler, problem çözme veya tahminlerde bulunmayla ilgili belirsizlikleri anlamanın ve değerlendirmenin önemli olduğu konusunda geniş ölçüde hemfikirdir. Belirsizlikler arasında bir dengeye ve istenen kesinlik düzeyine ulaşmak çok önemlidir, çünkü çoğu bilim ve mühendislik girişimi, sorunun üstesinden gelmek için kullanılan bilgi, model ve çözümlerdeki belirsizliği kabul etmez. En genel ifade ile, aleatorik (rastlantısal) ve epistemik (sistematik) belirsizlikler olarak iki tür belirsizlik vardır. Aleatorik belirsizlikler, sürecin doğası gereği ortaya çıkan rastgele değişkenli belirsizliklerdir, daha fazla bilgi sağlanması ile azaltılamazlar. Epistemik belirsizlikler, teoride anlaşılabilir ancak pratikte tam

olarak doğrulanamayan faktörlerle ilişkilidir. Bunun nedeni, diğer nedenlerin yanı sıra belirli bir aşamadaki yetersiz bilgi veya veriler, belirli etkilerin göz ardı edilmesi veya ölçüm araçlarının hassasiyet sınırlamaları olabilir, daha fazla veri ve bilgi daha doğru ve kesin epistemik belirsizlik tahmini sağlar. Literatürde belirsizlik niceleme ve hassasiyet analizleri ile ilgili birçok farklı alanda çeşitli çalışmalar yer almaktadır. HAD araçlarının kullanımının artmasıyla eşzamanlı olarak, belirsizlik niceleme yaklaşımlarının HAD problemlerine uygulanması ile ilgili çalışmalar da hız kazanmaktadır. Literatürde kavitasyonun sayısal analizi ile ilgili çeşitli çalışmalar ve HAD problemleri üzerine uygulanan belirsizlik analizi çalışmaları çokça olmasına rağmen, bunları birleştiren; kavitasyon olgusu üzerinde sayısal belirsizlik analizinin yapıldığı çalışmalara rastlanmamıştır. Bu nedenle, mevcut tez çalışmasında kavitasyonun nümerik tahmininde girdi parametreleri ve ayrıklaştırma belirsizliklerinin ayrı ayrı ve birlikte incelenmesi üzerinde durulmuştur.

Pervane kavitasyonun üç boyutlu sayısal simülasyonu hesaplama maliyeti bakımından çok maliyetli olduğundan, bu çalışmada, parametre ve ayrıklaştırma belirsizliklerini tahmin etmek ve bunları tek bir değerde birleştirmek için test durumu olarak örnek bir iki boyutlu hidrofoil folyo üzerindeki kavitasyon davranışı araştırılmıştır. Seçilen test durumu, daha önce birçok araştırmacı tarafından deneysel olarak incelenen NACA 66 folyosudur. Bu test senaryosunun popülaritesi, deniz pervanesi tasarımıyla olan ilgisinden ve deneysel ve referans sayısal verilerin geniş kullanılabilirliğinden kaynaklanmaktadır. Girdi parametreleri olarak hücum açısı ve kavitasyon sayısı seçilmiş ve bunların kuvvet katsayıları, kavitasyon boyu ve kavitasyon hacmi gibi özellikler üzerindeki etkileri incelenmiştir. Çalışmanın ilk aşamasında, sabit tabaka kavitasyonuna karşılık gelen bir karakteristik koşul, mevcut deneysel veriler kullanılarak seçilmiştir ve bu nokta etrafında bir dizi simülasyon, HAD çözümünün hassasiyetini örneklemek için gerçekleştirilmiştir. Çalışmada yapılan tüm simülasyonlarda Hollanda Denizcilik Araştırma Enstitüsü'nün (MARIN) şirket içi kodu olan ReFRESCO kullanılmıştır. Elde edilen sonuçlar, giriş parametrelerinin ve ızgara yoğunluğunun kavitasyon özellikleri üzerindeki etkisini araştırmak için belirsizlik niceleme (UQ) prosedürüne tabi tutulmuştur. Girdi ve ayrıklaştırma belirsizliklerinin göreli önemini ölçmek için Sobol endeksleri de elde edilmiştir. Ayrıca, ayrıklaştırma belirsizliğinin çıkış parametreleri üzerindeki etkisini araştırmak için üçüncü girdi parametresi olarak ayrıklaştırma belirsizliği ele alınmıştır.

Sobol yöntemi, her bir girdi parametresinin ilgili çıktı parametresi üzerindeli toplam katkısını ve bunların çıktının varyansına olan etkileşimlerini hesaplamayı mümkün kılan bir yaklaşımdır. Sobol yönteminde, modelin çıktı parametrelerindeki değişimin ne kadarının tek bir parametrenin değişmesinden veya farklı girdi parametreleri arasındaki etkileşimden kaynaklandığının belirlenmesi amaçlanmaktadır. Girdi parametrelerinin seçimi ve değişikliğin nedenleri vurgulanmaz, yalnızca girdi parametrelerindeki değişikliklerin çıktı parametreleri üzerinde ne ölçüde etkili olduğu vurgulanır. Bu adımda, daha önce MARIN' de gerçekleştirilen bir çalışmada geliştirilen ve geçiş bölgesi Reynolds sayılarında kavitasyon yapmayan pervanelere ve düz plakalara uygulanan metodolojiden yararlanılmıştır.

Deney Tasarımı (DoE), ister HAD çözümlerinden oluşan bir varlık, ister açık bir matematiksel işlev olsun, bir işlevi metodik ve verimli bir şekilde örneklemek

için kullanılan istatistiksel yaklaşımları ifade eder. Bu çalışmada deney tasarımı olarak Latin Hybercube Örneklemesi (LHS) ve vekil model yaklaşımı kullanılmıştır. Belirsizlik niceleme çalışmalarında örnekleme yönteminin kullanılması, çok sayıda numune noktasına ihtiyaç duymaktadır. Gerçekleştirilen simülasyonlar iki boyutlu olmasına rağmen, her ızgara iyileştirme seviyesinde çok sayıda hesaplama gerçekleştirmek hesaplama maliyetini de önemli ölçüde arttıracaktır. Bu nedenle bir vekil model kullanımı tercih edilmiştir. Vekil modeller (aynı zamanda meta-model veya yanıt yüzeyi yaklaşımı olarak da adlandırılır), bir deneyin veya simülasyonun sonuçlarına yaklaşan bir fonksiyondur ve verileri üretmek için orijinal olarak kullanılan yaklaşımdan hesaplama açısından daha ucuzdur. Bu yaklaşımda, belirsizlik niceleme analizi için ihtiyaç duyulan çok sayıda numuneyi örneklemek yerine, daha az sayıda numune ile oluşturulan verilerle uygun bir yüzey tanımlanmıştır. Çalışmanın ilk aşamasında valide edilmiş örnek değerler baz alınarak girdi parametreleri için belirli aralıklar belirlenmiş ve bu aralıklardan toplamda 25 örnekleme noktası içerecek bir örnek uzayı oluşturulmuştur. Yalnızca bu noktaların HAD simülasyonları gerçekleştirilmiştir. Daha sonra elde edilen sonuçlardan vekil model yaklaşımı kullanılarak çıktı parametrelerinin her biri için ayrı ayrı yanıt yüzeyleri oluşturulmuştur. Belirsizlik niceleme analizi için daha sonra bu yanıt yüzeylerinden 2^{11} ile 2^{16} aralığında nokta sayısı kadar nokta çekilmiş ve Sobol indisleri kontrol edilmiştir. Sobol indislerinin daha hassas hesaplanabilmesi için 2^{15} nokta sayısının yeterli olduğu görülmüştür ve bu değerle hesaplamalara devam edilmiştir.

Elde edilen sonuçlar, sürükleme katsayısı (C_D) ve kavitasyon uzunluğu (L_{cav}) gibi girdi parametreleri için güven aralıkları ve Sobol endeksleri, ızgara iyileştirmesindeki değişikliklere rağmen çoğunlukla değişmeden kaldığını; bu çıktı parametreleri için parametre belirsizliklerinin baskın faktör olduğunu göstermektedir. Kaldırma katsayısı (C_L) ile ilgili olarak, ayrıklaştırma belirsizliğinin etkisinin C_D ve V_{cav}'den daha büyük olduğu ancak, yine de parametre belirsizliğinin ayrıklaştırma belirsizliğinden daha önemli bir etkiye sahip olduğu gözlenmiştir. Diğer çıktı parametrelerinin aksine, kavitasyon hacmi (V_{cav}) parametresi için alınan sonuçlar, bu parametre üzerinde ayrıklaştırma belirsizliğinin parametre belirsizliğinden daha büyük bir etkiye sahip olduğunu göstermiştir. Bununla birlikte, çalışma yine de parametre belirsizliğinin bu çıktı parametresinin belirlenmesinde önemli bir rol oynadığını göstermiştir.

Bu çalışmanın kapsamını genişletmek için gelecekteki araştırmalarda, bu çalışmada sunulan analiz çerçevesini kullanarak zamana bağlı -kararsız- akış uygulamaları için ayrıklaştırma ve girdi belirsizliğini ölçmenin yanısıra iteratif belirsizliğin veya zaman adımı belirsizliğinin etkilerini de göz önünde bulunduran bir formülasyon geliştirilebilir. Türbülans veya kavitasyon modelleriyle ilgili katsayılar gibi diğer parametreler, ağ ve çalışma noktası koşullarına ek olarak modelleme belirsizliklerinin ek derecelerini hesaba katmak için analizlere dahil edilebilir.

1. INTRODUCTION

1.1 Overview of Cavitation

Cavitation is a physical occurrence observed in liquid flow, where the pressure falls below the vapor pressure, resulting in the creation and eventual implosion of vapor bubbles [1]. It is a common occurrence in many engineering systems, including hydraulic machinery, pumps, and marine propellers [2]. Cavitation has important influences on fluid systems, it can lead to erosion of material surfaces due to the high-speed collapse of bubbles, it can cause noise and vibrations that can damage or effect efficiency of the system.

1.2 Importance of Understanding Cavitation for Marine Propellers

The presence of cavitation in marine propellers is a critical problem that can drastically reduce propeller efficiency whilst causing erosion of the blade surface and increasing the generated noise and vibrations. The accurate prediction of cavitation requires an understanding of the physical mechanisms involved and the use of appropriate numerical models to simulate the complex flow phenomena [3]. Experimental methods, including visualization techniques and performance testing, are also commonly used to study cavitation on marine propellers [4]. While cavitation is an essential phenomenon to consider in the early design stages of a ship, predicting propeller cavitation behavior numerically remains challenging. The primary reasons for this are the computational expense and constraints of current numerical models. Furthermore, uncertainties associated with boundary condition values, modeling constants, grid density, and time step size have not been fully understood.

To summarize, comprehending cavitation effects on propellers is crucial owing to its potential implications for vessel safety and efficiency. Accurate prediction and mitigation of cavitation on marine propellers require a combination of physical

understanding and numerical modeling techniques, along with experimental validation [2]–[7].

1.3 Content and Purpose of This Thesis

The main aim of this study is to address these issues by applying uncertainty quantification techniques to CFD simulations of cavitation using Maritime Research Institute Netherlands (MARIN)'s in-house code, ReFRESCO[1]. Cavitation behaviour on a 2D hydrofoil is investigated. The chosen test case is the NACA 66 foil studied experimentally by [8] and other authors. The popularity of this test case stems from its relevance to marine propeller design and the wide availability of experimental and reference numerical data. An example cavitating flow for this foil is depicted in Figure1.1. A characteristic condition corresponding to steady sheet cavitation has been selected using the experimental data available and a series of simulations around that point have been carried out to sample the sensitivity of the CFD solution. Subsequently, the results were subjected to UQ procedure to investigate the influence of input parameters and grid density on cavitation characteristics. This step took after the methodology previously developed by [9] and applied to non-cavitating propellers and flat plates at transitional Reynolds numbers.

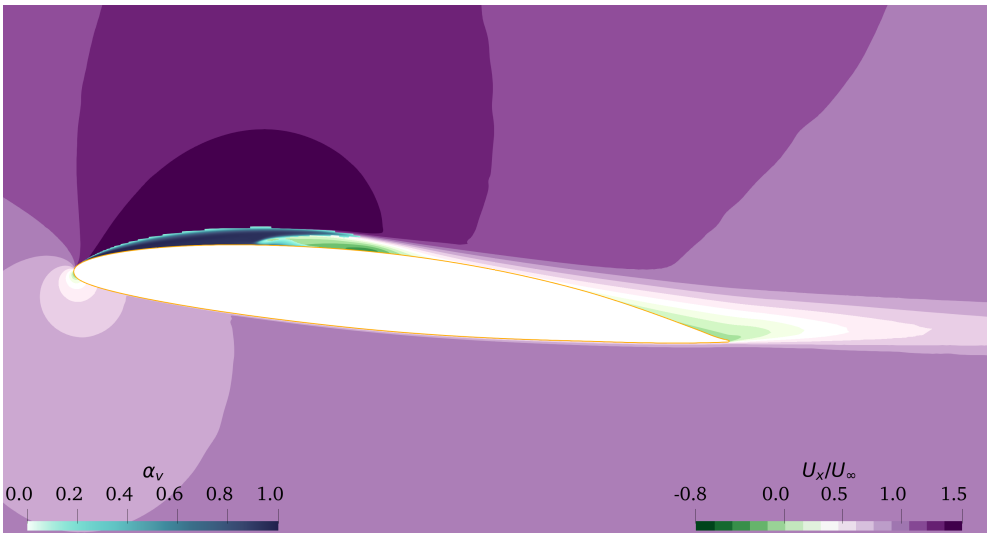

Figure 1.1 : Overview of the vapour volume fraction (α_v) and streamwise velocity around the considered NACA 66 foil. Conditions mimic those of the experimental study of [8] at 6 degrees angle of attack.

[1] https://www.marin.nl/en/facilities-and-tools/software/refresco

2. LITERATURE REVIEW

2.1 Studies on Propeller Cavitation

Cavitation is generally defined as a phenomenon resulting from a pressure drop, which causes a type of cold-boiling effect. This occurrence is likely to happen in any mechanical system that includes liquid fluid. Hydrodynamic cavitation is the most frequent form of cavitation in engineering, and it involves motion. Examples of hydrodynamic cavitation can be found in various mechanical systems, such as impeller flow, narrow channel flows like hydraulic valves, flows through venturi nozzles, and volumetric pumps used for fuel injection in engines. The maritime industry is mainly concerned with cavitation issues associated with rudders, hydrofoil boat legs, and the various types of propeller cavitation. Lifting surface methods, panel methods and computational fluid dynamics (CFD) methods are used to numerically analyze cavitation in lifting surfaces such as hydrofoil and propeller used in the marine field. Research has indicated that the outcomes attained from the aforementioned analysis techniques are of such a caliber that they can substitute the outcomes achieved through experimental methods and result in savings with regard to both time and expenses.

A study was carried out by Gindroz and Billet [10] to examine the influence of nuclei size on initiation of the cavitation for diverse forms of cavitation on ship propellers. They based their analysis on both their own experiments and previous tests and studies documented in the literature. Mueller and Kinnas [11] utilized the finite element method to investigate the cavitation analysis of a propeller that was functioning in an axisymmetric flow. They developed an algorithm that can anticipate the point where the cavitation will separate in the wing section. The theoretical findings were authenticated by comparing them with the results obtained from experiments conducted at MIT, and it was observed that the outcomes were coherent. Yuka Iga et al. [12] numerically calculated the two-dimensional unsteady cavitation flow on

hydrofoils arranged in layers. A homogeneous model of a compressible two-phase gas-liquid medium was applied to analyze the cavitation current. From the numerical results obtained, it was seen that there are at least two mechanisms in the separation event of the layer cavitation. The first of these mechanisms is that the re-entrant jet contributes to the detachment of cavitation, the second one is that the propagating pressure waves and cavitation surface waves cause the emergence of a distinct type of separation phenomenon. In their study, Kinnas et al. [13] used the lifting surface and panel method to solve the unsteady cavitational flow around a propeller operating in an axially symmetrical environment and found that unsteady layer cavitation occurs very commonly on ship propeller blades. The length and thickness of the cavitation layer, which changes depending on time, and the location of the separation point of the cavitation layer were determined by iterative methods. The outcomes acquired via the two approaches were contrasted with the experimental findings. A study conducted by Vaz G. et al. [14] revealed their discoveries on the creation of a three-dimensional panel methods, which was designed to analyze cavitating ship propellers and the mathematical model theory of layer cavitation. Both permanent and non-permanent cavitational flows were examined to validate the accuracy of the method. To evaluate the accuracy of the non-cavitating flow, numerical outcomes were compared against an analytical solution on an ellipsoidal structure. To examine the cavitating current, the number of grids in the numerical model was increased, and the pressure distributions were verified using the DTMB P4119 propeller. Two propellers were utilized to compare the numerical results with experimental data in open water conditions. Upon concluding the investigation, the experimental results of both propellers were compared at various propagation coefficients and cavitation numbers, and the computed cavitation patterns were found to be consistent. Coutier-Delgosha et.al [15] conducted research into the dynamic characteristics of cavitation using both experimental and numerical approaches. In the experiments conducted at the ENSTA Paris Tech cavitation tunnel, they investigated the influence of different flow conditions such as pressure, flow velocity, and attack angle of the foil on the cavitation dynamics. More precisely, they examined the layer at the rear of the two-dimensional foil section to understand the unsteady nature of the cavitation flow.

The researchers compared the numerical outcomes with the experimental findings. E.J. Foeth et al. [16] utilized the time-resolved PIV technique to investigate fully developed layer cavitation on a hydrofoil, aiming to identify the three-dimensional cavitation patterns that lead to negative effects such as vibration, noise, and erosion. Their findings showed that the velocity at the cavitation interface was consistent with the predicted simple streamline model velocity. By analyzing time-resolved recordings, they traced the development of bound cavitation and cloud scattering. The researchers concluded that their PIV measurements for enhanced layer cavitation were precise, based on the results of their research. J.A. Szantyr [17] reviewed four contemporary computational fluid mechanics methods used in ship hydrodynamics: the lifting surface method, boundary element method, RANS method, and Large Eddy method. The focus was on how these methods were applied in the last four years to determine propeller geometry and design procedures. Szantyr also discussed important issues such as identifying the vortex impeller and predicting different cavitation forms and their hydrodynamic effects. Examples were provided to illustrate these points. R. Arazgaldi et al. [18] investigated ship propeller cavitation experimentally and numerically. For this study, two different types of classical model propellers, one with four blades and the other with three blades, were used. Various cavitation regimes were investigated for the four-bladed propeller using a cavitation tunnel. Three-bladed propeller, based on available experimental results; A two-dimensional NACA0015 hydrofoil was subject to numerical investigation to study the cavitation occurance. The outcomes were consistent with the experimental findings, for both cavitating and non-cavitating conditions. Van et al. [19] performed experiments using a propeller model in MARIN's Depressurized Towing Tank. The model was tested thoroughly beforehand and tested under varying dissolved gas and free-stream nuclei contents. They presented a conceptual model to clarify sheet cavitation inception and account for the experimental results. The outcomes demonstrated that achieving sheet cavitation inception on propeller models requires both leading edge roughness and adequately small free-stream nuclei. Subhas et al. [20] studies with a complete computational solution for the determining performance of a propeller opereting in cavitating condition, utilization of the CFD tool Ansys Fluent. They validate the

results of open water characteristics of the propeller with the experimental predictions. Pail et al. [21] conducted simulations of cavitation and hull pressure surge resulting from a propeller operating in aft of a ship, using the Unstable Reynolds-Averaged Navier-Stockes (URANS) approach with Fluent, a commercial CFD code. To model the ship's wake field in the propeller plane, they simulated a full hull submerged beneath the free surface, while a symmetry boundary condition was applied to the top of the computational field in place of the free surface, similar to cavitation tunnels. The sliding mesh technique was used to rotate the propeller and observe the cavitation pattern. By running simulations at two different draft values, they investigated the impact of the cavitation number. The technique was verified through two distinct propeller simulations. The outcomes were matched with those of experiments performed in the Samsung Cavitation Tunnel (SCAT), demonstrating good consistency. Lee et al. [22] proposed an analytical source model for sheet cavitation and a multi-parameter inversion scheme to determine the locations of noise sources and their intensities, and applied this technique to analyze hull pressure data obtained from a cavitation tunnel at Samsung Heavy Industry. The findings revealed that only two monopole sources were necessary to represent the propeller sheet cavitation noise and that the inverted source data aligned well with the propeller's cavitation dynamics. Additionally, the modeled hull pressure demonstrated good agreement with the experimental data obtained from the cavitation tunnel. Aktas et al. [23] conducted experiments on cavitation in a medium-sized cavitation tunnel to gather data on the Underwater Radiated Noise (URN) of a full-scale vessel. The goal was to assess the prediction methodology and compare the extrapolated URN data from the tunnel tests to the data obtained from full-scale trials. According to the findings, although testing a full-hull model in large cavitation tunnels is the best approach, the use of medium-sized facilities with dummy-hull models and wake screens can still yield valuable insights for studying URN. Helal et al. [24] described a comprehensive and detailed process for simulating cavitating flow on marine propellers using the $'K-Kl-\omega'$ transition-sensitive model, using cfd code Ansys Fluent. They adopt the fully turbulent standard $'k-\varepsilon'$ model to compare the results. The data obtained from both turbulence models are then validated by comparing them with

experimental data available in the literature. The results showed that the predictions based on the $'K-Kl-\omega'$ transition-sensitive model are more accurate at lower rotational speeds, specifically at low Reynolds numbers. Bosschers [25] discussed the tip-vortex cavitation which causes of broadband pressure and hull fluctuations, reason of the underwater radiated noise. Melissaris et al. [26] examined the impact loads of cavitation on a propeller surface by utilizing a URANS approach. Their findings indicated that by estimating the vapor volume reduction rate through the use of the mass transfer source term, the conservation of energy was ensured, resulting in a fulfilled total energy balance. After testing the model on a single cavitating bubble collapse, they proceeded to validate it using a model propeller test case. The resulting surface impact distribution closely matched that of the experimental paint test, demonstrating the potential for the fully conservative method to accurately forecast cavitation implosion loads on propeller blades.

2.2 Studies on Uncertainty Assessment in CFD Simulations

Regarding the utilization of UQ in CFD simulations, uncertainties related to the input parameters such as material features, or initial-boundary conditions are referred as aleatoric uncertainties due to they have random effects in some cases; Uncertainties related to the parameters not known precisely are referred as epistemic uncertainty [9]. Uncertainties encountered in the input parameters mean that there are also uncertainties in the output data obtained as a result of the simulations. Therefore, UQ analysis is applied to determine and estimate the uncertainties that have an effect on the outputs by studying and quantifying the effect of the uncertain input variables.

Generally, UQ analysis methods are studied by two main approaches as intrusive and non-intrusive methods. Herzog et al. [27] compare the intrusive and non-intrusive methods for computing Polynomial Chaos expansions and performed an efficiency and accuracy analysis by applying the Polynomial Chaos expansion to a practical problem in the field of stochastic Finite Elements. A spectral decomposition of random variables and other random quantities, including but not limited to polynomial chaos methods, are introduced by Sullivan [28]. In order to determine the coefficients in spectral expansions, the intrusive (stochastic Galerkin method) approach is discussed

in addition to the alternative non-intrusive (sample-based) paradigm. These are applied to probability-based UQ. An UQ scheme which combines a Galerkin approach procedure for the determination of polynomial chaos coefficients with a projection method has been developed by Le Maitre et al. [29,30]. Xiu et al. [31] presented a new algorithm which can be considered as a generalized form of the original polynomial chaos expansion, in order to model the input uncertainty and its propagation in incompressible flow simulations and applied it to micro-channel flows. Mathelin et al. [32] discuss the Polynomial Chaos and Stochastic Collocation approaches in order to compute the propagation of uncertainty in numerical simulations in the specific context of a quasi-one-dimensional nozzle flow with uncertainty in inlet conditions and nozzle shape. Onorato et al. [33] discussed and compared the effects of intrusive and non-intrusive polynomial chaos expansion methods on the quality of results of CFD simulations of a trans-sonic RAE2822 airfoil. Hirsch and Dinescu [34] implemented the intrusive polynomial chaos methodology to a CFD case by using the FINE/Turbo commercial solver and subjected to a verification and validation program. Phillips and Roy [35] presented a new uncertainty estimator for CFD applications based on Richardson extrapolation. It utilizes global order of accuracy and assorted metrics to calibrate and appraise the uncertainty estimator. Cuneo et al. [36] applied four Monte uncertainty quantification methods, namely Monte Carlo, Polynomial Chaos, Mid-range Approximation, and a combined Monte Carlo and Polynomial Chaos method, to multiple analytical test functions and engineering test cases. The assessed the engineering problems includes many stochastic design parameters and discussed the strengths and weaknesses of the four methods. Although there are has been a substantial amount of research effort dedicated to making the Stochastic Galerkin method easier to use, doing so still poses challenges.

Researchers are choosing the non-intrusive approaches due to not only using a computational model is easy and adventageous but also Galerkin method has the possibility of expeditiously increase in the computational cost with the number of random dimensions [9,37]. However, in practice, the large number of samples typically required in the sampling-based approach can greatly increase the computational cost

of CFD simulations. In the present study, the non-intrusive approach is coupled with a surrogate model of the CFD solution in order to overcome this issue.

Although there are numerous studies in the literature on Cavitation phenomenon and UQ in CFD Simulations conducted seperately, to my knowledge there is no study dealing with uncertainty quantification in the numerical prediction of cavitation. With this in mind, this thesis study focuses on the quantifying uncertainties on dynamic cavitation phenomenon.

3. CAVITATION

3.1 History of Cavitation

Cavitation was first observed in waterwheels during the early 1700s, marking the beginning of its history. Leonhard Euler, a French mathematician and physicist, described cavitation in 1754 when he wrote about the vacuum phenomenon in fluids. He noticed that when water flowed over blades of a wheel, it would boil, forming small bubbles that collapsed and damaged the blades. In the 1800s, Carlo Marangoni, an Italian physicist, delved deeper into the cavitation phenomenon and formulated equations to explain its behavior. He discovered that bubble formation and collapse could result in strong shock waves that could cause surface damage. In 1873, Osborne Reynolds wrote articles on propeller steam engines which revealed what we now call cavitation in marine engineering. In the late 19th century, there was a goal to create faster ships, with the first trial taking place on the British destroyer "Daring" in 1894. However, the ship only reached 24 knots instead of the targeted 27 knots due to flow distortions, leading to the phenomenon being named "Cavitation" by R.E. Froude's suggestion, derived from the Latin word "Cavus". In 1895, Charles Parsons observed cavitation during the trials of the "Turbinia" and invented the first cavitation tunnel, which tested small propellers. This tunnel had a 2-inch diameter limitation, leading to Parsons building a larger tunnel 15 years later to test 12-inch diameter propeller models. Parsons used a vacuum pump to reduce atmospheric pressure above the water level in the tunnels, enabling observation of cavitation at low shaft speeds. From the 1920s to the early 1930s, bigger cavitation tunnels were constructed in both Europe and America. Since then, numerous investigations into cavitation have been conducted using both experimental methods in cavitation tunnels and numerical models, and such studies continue today. The advancement of computer technology from the 1950s has led to significant progress in this area. Cavitation remains a crucial subject of exploration within fluid dynamics, with practical uses in various fields such

as engineering, physics, and biology. Scientists persist in examining the properties of bubbles and the impact of cavitation on diverse materials, while also inventing fresh technologies to mitigate the effects of cavitation across multiple applications.

3.2 Basic Physics of Cavitation

The fundamental mechanism that controls the process of cavitation can be seen as a variation of the commonly known situation where water boils at a higher temperature in lower altitudes. During cavitation, the pressure decreases while the temperature remains constant, such as the temperature of the surrounding seawater in the case of a propeller. If inception of cavitation were when the local pressure reaches the fluid's vapor pressure, then the cavitation number sigma at the point of inception would be equivalent to the minimum pressure coefficient Cpmin. Nonetheless, several additional factors exist that prevent the straightforward correlation from being applicable. These factors include the fluid's capacity to endure stresses, the requirement for nuclei to have a specific residence period in order to reach a measurable size, and the typical usage of measurement and computation methods that generate time-averaged pressure coefficient values.

The phenomenon of cavitation is also described as a form of cold-boiling. To understand this, the water phase diagram shown in Figure 3.1 can be examined. As seen in the diagram, in order to turn liquid water into gas form under constant pressure, the temperature should be increased (from point B to point A). However, at the same time, while keeping the temperature constant, by reducing the pressure (from point C to point A), it can be ensured that the liquid water turns into gas form. It is crucial to comprehend the distinction between the two types of evaporation referred to. TThe familiar process of evaporation takes place when a state transition occurs due to an increase in temperature along a flat surface that separates the liquid and its vapor. The associated shift in vapor pressure is temperature-dependent, and the vapor and its liquid can remain in equilibrium along this curve. The second situation in which phase change occurs with pressure drop is cavitation, where air voids are formed in the liquid.

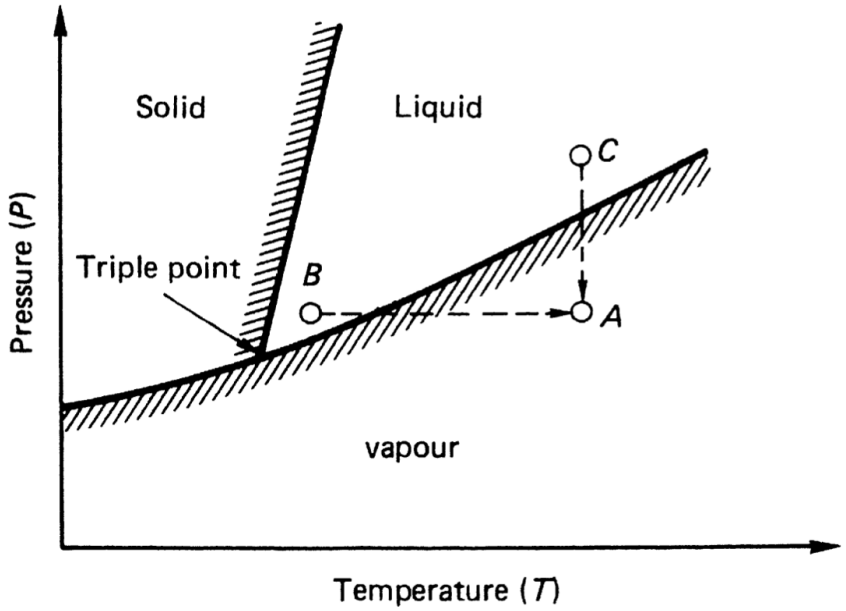

Figure 3.1 : Phase diagram for water [38].

3.3 Mathematical Modeling of Cavitation

Cavitation models are utilized to predict the occurrence and extent of cavitation in fluid flow. There are various types of cavitation models. Homogeneous models consider the vapor-liquid mixture as a single-phase medium, while bubble dynamics models examine the behavior of individual vapor bubbles and their interactions with the surrounding fluid. Two-phase flow models take into account the interaction between the vapor and liquid phases, while energy-based models utilize energy conservation principles. The selection of a cavitation model depends on the specific application and desired accuracy. Advanced numerical simulations can aid in the calibration and validation of cavitation models and enhance the understanding of the physics behind cavitation. In general, modelling attempts of cavitation can be classified mainly as vapor transport based modeling and discrete bubble dynamics based modeling.

3.3.1 Vapor-Transport models

They are most appropriate for analyzing cavitation that occurs on a large scale, such as sheet cavitation that frequently appears on rudders and propellers. These models involve double-sided interactions among the phases.

3.3.1.1 Two-Phase models

Involves the representation of two distinct phases, such as free surface consideration. Two commonly used models for simulating multiphase flows are homogeneous mixture models and sharp interface models, which have distinct approaches in handling cells containing both phases.

Homogeneous Mixture models

This method assumes that the ingredients inside each cell has a uniform composition, making it best suited for modeling numerous small bubbles that are much smaller than a cell. However, this approach has a drawback: When the cavitation voids are larger than a single cell, the vapor fraction diffuses into adjacent cells via the vapor transport pattern. Despite this limitation, most modern cavitation models rely on homogeneous mixing models.

- Singhal et al. Model

  Singhal et al. [39] developed a model that builds upon the "full cavitation model" and incorporates all significant first-order effects, including bubble dynamics, phase change, turbulent pressure fluctuations, and non-condensable gases. The model is capable of considering multiphase flows or flows where multiple phases are being transported, accounting for shear rates between gas and liquid phases, and the thermal and compressibility effects of both phases. However, this model is only compatible with the multiphase mixture model and necessitates the primary phase to be liquid and the secondary phase to be vapor.

- Zwart-Gerber-Belamri Model

  It is developed by Zwart-Gerber-Belamri [40] an the rate of change in density and mass of a single cavitation bubble is taken into account by it, assuming that all bubbles produced during cavitation have a uniform size.

- Schnerr and Sauer Model

  It is a model developed by Schnerr and Sauer [41] that is similar to Singhal's model in its approach to calculating the net mass transfer from liquid to vapor. Unlike the

previous two models, Schnerr and Sauer employ an alternative equation to link the vapor volume fraction to the density of bubbles per unit volume of liquid. In this model, only the density of spherical bubbles per unit volume of liquid needs to be determined. If no new bubbles are formed or eliminated, the density of bubble stays unchanged, and only the starting values of the nucleation place volume fraction and the balance bubble radius are required to define the bubble number density. Further details and mathematical formulas are available in [41].

Sharp Interface models

Sharp interface models preserve a clear distinction between the two phases and do not diffuse the interface by advection, which is suitable for scenarios where the bubble size is relatively large, typically equivalent to or greater than a few cells.

3.3.1.2 Phase-Change models

Mass transfer among two various phases are involved in this models. Unlike boiling, mass transfers between liquid and vapour in cavitation are driven not by temperature but by pressure. For this reason, pressure is in the foreground for this models utilized for cavitation modelling. Two primary categories of phase change models are commonly used in cavitation analysis, namely barotropic models and equilibrium models.

Barotropic Model:

It assumes that the fluid undergoing cavitation is barotropic, meaning that the pressure is solely a function of the density of the fluid and the bubbles are in thermodynamic equilibrium with the surrounding liquid. It also assumes that the bubbles are spherical and non-interacting. It may not be accurate for systems where the fluid is not barotropic, such as compressible fluids or fluids undergoing chemical reactions.

Equilibrium Model:

The energy equations are taken into account in this cavitation model. The amount of energy obtained or spreaded during the phase change of the fluid is taken into account.

3.3.2 Discrete Bubble models

The discrete bubble cavitation model treats vapor bubbles as individual entities and utilizes a set of equations to determine their behavior regarding growth and collapse. This model assumes that vapor bubbles are sufficiently spaced apart and do not interact with each other. It is widely used in simulating cavitation in pumps and marine propellers, providing a comprehensive analysis of the cavitation process on a microscale level.

3.3.2.1 Rayleigh Model

It is the oldest cavitation model dates back to 1917. It was formulated by Lord Rayleigh [42], who proposed a model that describes a void within the fluid influenced by an unchanging external pressure. Because the model assumes the presence of an empty space, it is commonly referred to as a "cavity."

3.3.2.2 Rayleigh-Plesset Model

Plesset expanded on Lord Rayleigh's work by introducing the Rayleigh-Plesset cavitation model. This model incorporates additional factors such as viscosity, surface tension, and an unsteady external pressure into Lord Rayleigh's original equation.

3.3.2.3 Gilmore Model

Gilmore's equation takes into accounts for how much the liquid can be compressible, but the derivation of the equation neglects the contribution of viscosity since the viscous term only appears as a product with compressibility.

3.4 Cavitation in Marine Propellers

Propeller cavitation is a crucial issue faced in the maritime industry, particularly in high-speed ships. When the propeller rotation rate is high, pressure in the liquid drops below its vapor pressure, causing the formation of vapor bubbles. These vapor bubbles can occur in different locations and shapes and lead to different types of cavitation, such as sheet, sheet, cloud, bubble, face, root, vortex-type cavitation shown

in Figure 3.3. Each type of cavitation can have different effects on the propeller propeller performance and efficiency, as well as the ship's overall performance; or can damage the structure of propeller such as in Figure 3.2. Therefore, understanding the mechanisms of propeller cavitation and developing efficient mitigation techniques are crucial for the safe and reliable operation of ships.

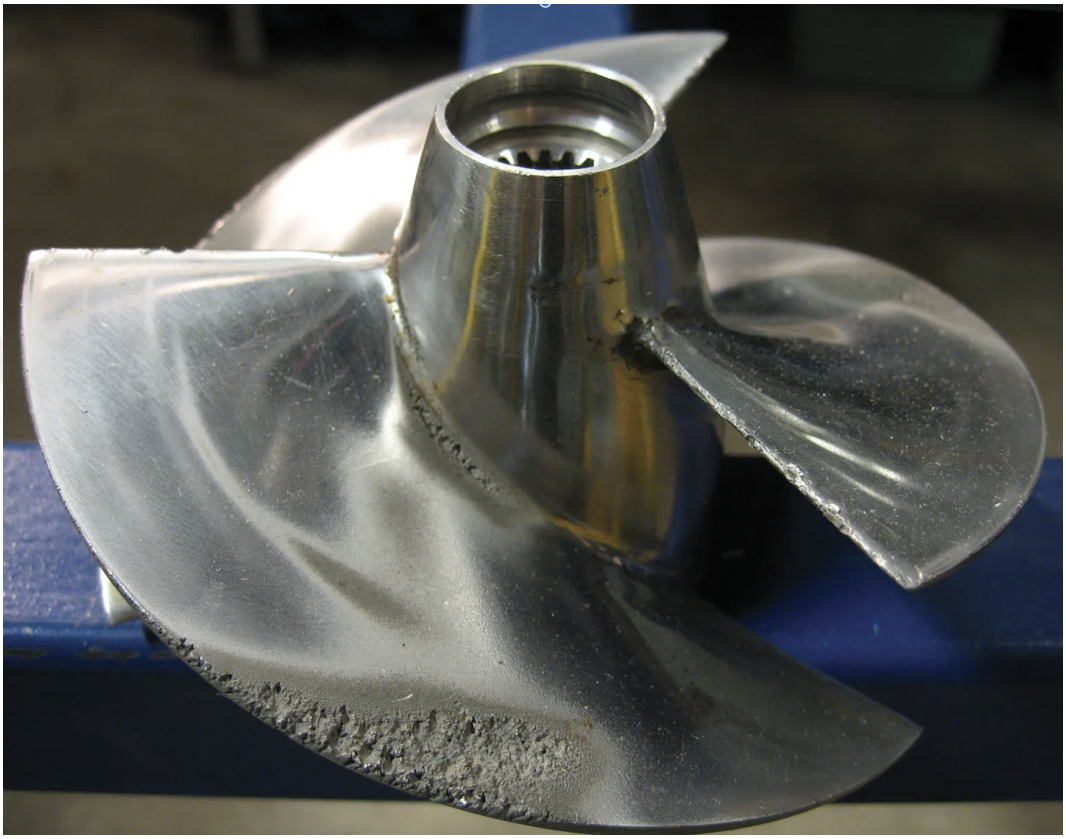

Figure 3.2 : Cavitation-induced propeller damage [43].

3.4.1 Types of propeller cavitation

3.4.1.1 Sheet cavitation

The manifestation of sheet cavitation usually occurs at about the foremost edges of propeller blades on the back side of the blade surface, particularly if the sections are functioning at positive incidence angles. However, when functioning at negative incoming angles, it may start initially on the face (pressure) side surfaces of the blade. As the magnitude of the incidence angles increases or the cavitation number decreases, the size of the cavitation on the blade will increase both in the chord direction and in the radial direction. Usually, sheet cavitation is stable in nature, although there may be

situations where some degree of instability can be detected. It can be reduced by using materials that are more resistant to cavitation or by changing the blade geometry [44].

3.4.1.2 Cloud cavitation

Cloud cavitation often occurs in the wake of well-established and stable sheet cavities, particularly in flow conditions where moderate separation occurs and small vortices create small cavities and bubbles are distributed randomly across the blade surface of the propeller. The visual appearance of cloud cavitation is characterized by a collection of tiny bubbles that resemble a mist or cloud. It can be reduced by increasing the blade area or changing the blade geometry [45].

3.4.1.3 Bubble cavitation

The main factors that affect bubble cavitation are the pressure components that create high suction pressures in the mid-chord region of the blade sections. Therefore, the pressure distributions of the camber line and section thickness have a significant impact on a propeller's tendency to experience bubble cavitation. It usually emerges initially in the mid-chord area of the blade in non-separated flows. It manifests as individual bubbles that rapidly grow and contract over the blade surface, and can sometimes be quite substantial. The repeated collapse of bubbles can cause erosion or pitting of propeller blade surfaces, leading to failure or reduced efficiency.

3.4.1.4 Face cavitation

The occurrence of face cavitation happens on the propeller's driving face (pressure side) and can be caused by an improper pitch distribution across the blade's length, which results in a negative angle of attack and too small of a tip pitch. This type of cavitation is commonly seen on controllable pitch units and can cause severe damage.

3.4.1.5 Root cavitation

It occurs at the root of the propeller blade and is wedge-shaped. If the circulation around the propeller root is strong enough to cause erosion damage to the boss, root cavitation can occur at different points in the propeller's rotation. When the root

vortices move downstream past the propeller, they combine to form the boss vortex, which typically appears as a rope of bubbles with the same number of strands as the number of blades. On single screw vessels where the rudder is located behind the propeller, this bubble rope can collapse, leading to significant damage to the rudder post or leading edge of the rudder.

3.4.1.6 Vortex-Type (Tip and Hub) cavitation

The cavitation types associated with vortices typically happen at specific areas of the propeller, such as the blade tips, leading edge, and hub. While individual blade root vortices may not cavitate, the converging propeller cone increases their likelihood of cavitation. The resulting cavitation is generally stable and has a rope-like appearance that corresponds to the blades count. Tip vortex cavitation first appears behind the propeller blade tips and is characterized by the formation of a vortex that can be seen as a spiral trail behind the propeller and is initially unattached. Nevertheless, when the vortex intensifies, either because of an increase in load on blade or a reduce in cavitation number, it shifts towards the blade tip and becomes fixed. This type of cavitation typically occurs at high advance ratios and can lead to the formation of small vapor bubbles that are swept away by the flow. However, these small vapor bubbles can also cause significant noise and vibration. It can be reduced by increasing the blade area or changing the blade geometry [46].

3.4.1.7 Propeller-Hull Vortex (PHV) cavitation

In the early 1970s, Huse [47] identified a type of cavitation known as Propeller-Hull Vortex (PHV). This type of cavitation occurs when a cavitating vortex forms an "arc" between the blade tip and the hull. Tests conducted in a cavitation tunnel using flat plates placed above the propeller revealed that the propeller hull vortex type of cavitation is most prominent when there is only a small amount of space between the propeller's tip and the plates. Additionally, its incidence is significantly affected by the advance coefficient, with a higher likelihood of PHV cavitation occurring at lower advance coefficients. When the advance coefficient is small, the chances of PHV cavitation occurrence are more. The formation of propeller hull vortex is thought

to be a result of various flow disturbances and turbulence in the proximity of the hull, leading to a rotational movement around the stagnation point.The rotation away from the hull is intensified due to the small size of the control volume that shapes the vortex.

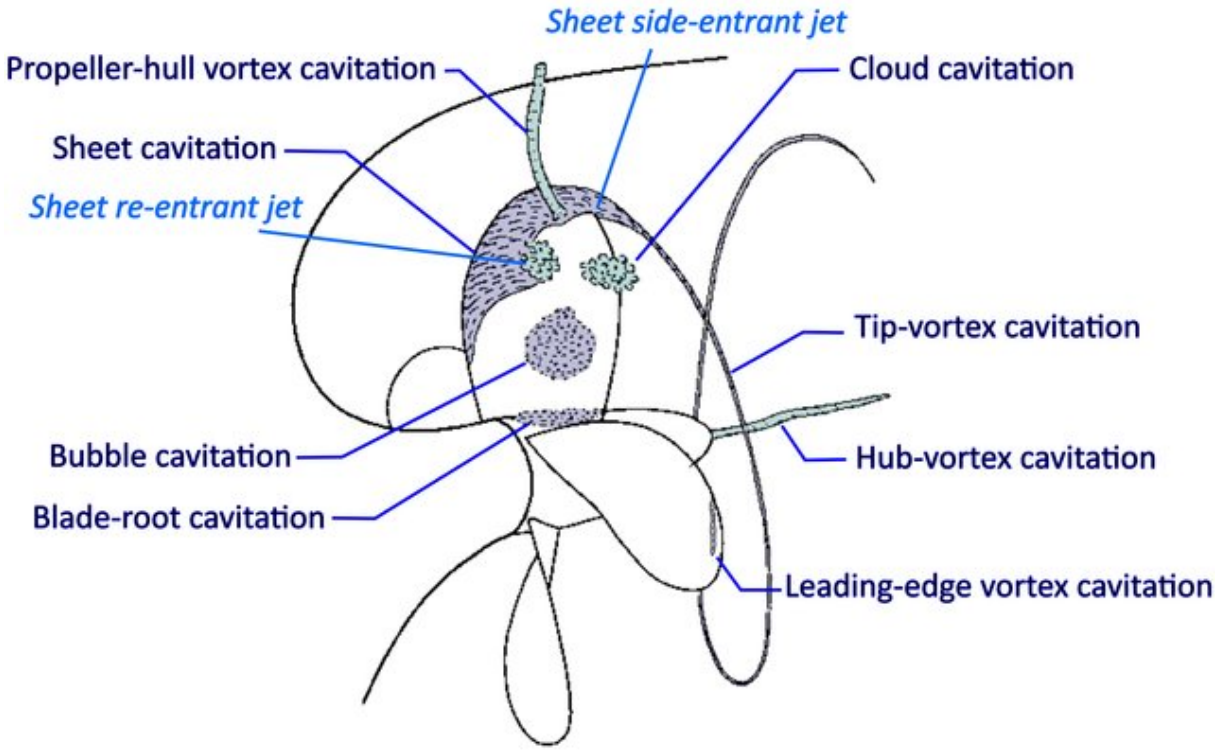

Figure 3.3 : Various types of cavitation patterns on ship propellers [48].

3.4.2 Cavitation consideration in propeller design

The complex environment of cavitation surrounding a propeller has a significant impact on both the intricate aspects of propeller design and the choice of propeller to be used [38]. The primary cavitation parameter implemented in the design of propellers is known as the cavitation number. Free stream-based cavitation number defined as:

$$\sigma_0 = \frac{p_0 - p_v}{\frac{1}{2}\rho v_A^2} \tag{3.1}$$

A diagram shown in Figure 3.4 serves as a helpful tool for beginners to choose the appropriate propeller type for a given application. In the diagram, it is seen that in which region of an operation area divided into zones according to the cavitation number (σ) and propeller advance coefficient (J) values, the use of conventional

or supercavitating type propellers is recommended. If neither conventional nor super-cavitating propellers are suitable for the design problem, alternative options such as waterjet or surface piercing propulsors should be considered to expand the range of propulsion choices.

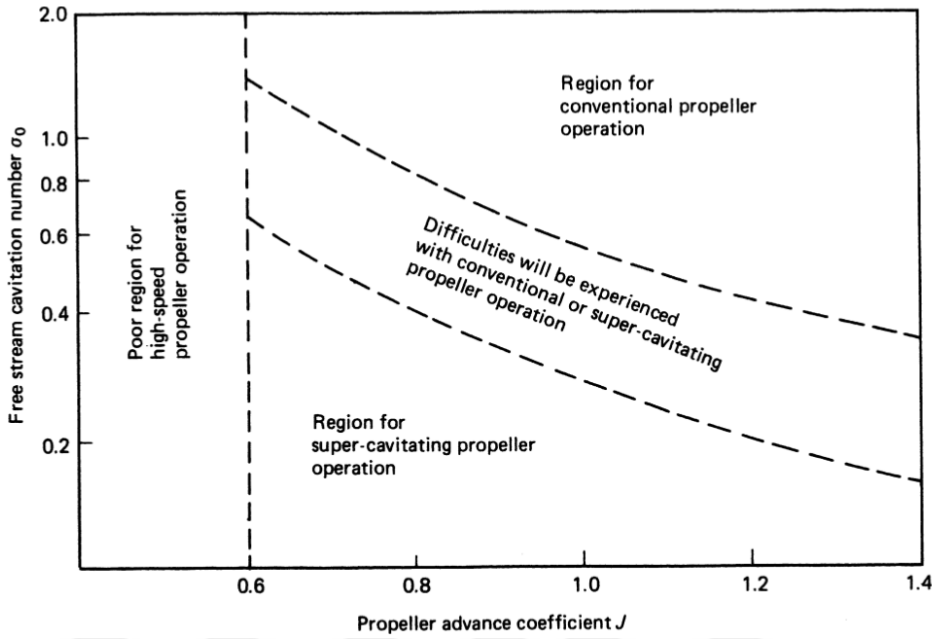

Figure 3.4 : Operation zones of marine propellers. (Prepared by Carlton [38] based on the studies conducted by Tachminji and Morgan [49]).

During the 20th century, many methodological studies were carried out for the control of cavitation during the propeller design stage, two of the most well-known are the Burril's [50] and Keller's [51] methods. The approach presented by Burrill focuses on the utilization of the diagram illustrated in Figure 3.5 and was intended for conventional propellers with a fixed pitch. The local cavitation number $\sigma_{0.7}$ calculated at 0.7R of the propeller blade and the thrust load coefficient τ_c which is calculated by using the projected area of the propeller blade, velocity at 0.7R of the blade and, the thrust produced by the propeller are used in the diagram. The suggested limitations according to type of vessels are seen in the diagram. The values denoting back cavitation percentages on the diagram are grounded on experiments conducted in a cavitation tunnel using a uniform axial flow.

The propeller blade projected area computed by employing the following formula using the value of τ_c obtained from the diagram:

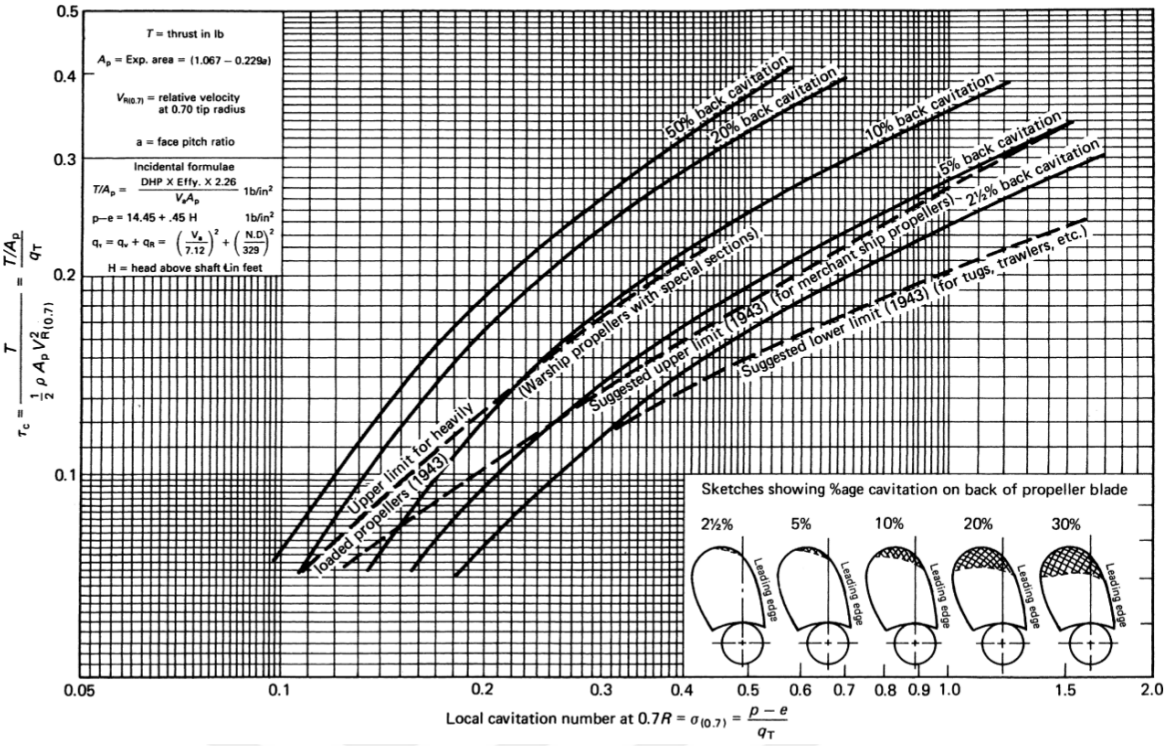

Figure 3.5 : Burril cavitation diagram for uniform flow [38].

$$A_P = \frac{T}{0.5\tau_c \rho [v_A^2 + (0.7\pi nD)^2]} \tag{3.2}$$

Burrill formulated an empirical equation to determine the expanded area from the projected area, but this relationship is applicable solely to conventional propeller shapes:

$$A_E = \frac{A_P}{1.067 - 0.229P/D} \tag{3.3}$$

Another blade area estimation propesed by Keller relies on the expanded area ratio relationship:

$$\frac{A_E}{A_P} = \frac{(1.3 + 0.3Z)T}{(p_0 - p_v)D^2} + K \tag{3.4}$$

In the quation, p_0 represents the static pressure at the shaft center line, p_v is the vapour

pressure (both are taken as unit kgf/m^2), T (kgf) is the thrust force produced by the propeller, Z is the blade count, and D is the diameter (m). The coefficient K given in the equation 3.4 takes different values depending on the ship type and the number of propellers, details can be found in [38].

4. UNCERTAINTY QUANTIFICATION

4.1 Overview of Uncertainties and Uncertainty Quantification

The term uncertainties can be defined in the simplest sense as 'things that are not known exactly'. Greater uncertainty in a problem results in reduced precision or reliability. It is widely agreed upon by analysts that it is important to comprehend and evaluate the uncertainties involved in solving problems or making predictions. Achieving a balance among uncertainties and the desired level of precision is essential since most scientific and engineering undertakings do not acknowledge the uncertainty present in the information, models, and solutions employed to tackle the problem [52]. Upon examining its historical context, it becomes evident that uncertainty, a situation that was traditionally deemed unacceptable in science, was not always acknowledged by the scientific community, despite its current significance [53]. The advancement of statistical mechanics has instigated a gradual trend within the scientific community over the past century to acknowledge and address the influence of uncertainty in problem-solving [52].

In general, there are two types of uncertainties: aleatoric (also known as stochastic uncertainty) and epistemic uncertainties. Aleatoric uncertainties are random variable uncertainties that arise due to the nature of the process while epistemic uncertainties, also known as systematic uncertainties, are associated with factors that are in theory understandable but not fully verifiable in practice. This may be due to inadequate knowledge or data at a particular stage, disregard of certain effects, or sensitivity limitations of measurement tools, among other reasons [28,54]. While aleatory uncertainties cannot be reduced with the further knowledge, more data and knowledge would allows for more accurate and more precise epistemic uncertainty estimation [55].

The procedure of measuring the uncertainties that arise from the model calculations of physical quantities of interest is termed as Uncertainty Quantification (UQ). Its key aims are to identify all relevant sources of uncertainty and evaluate the impact of specific sources on the overall uncertainty, as explained in [56]. Taking into account the uncertainty in our data and models, the Uncertainty Quantification process is a crucial tool that facilitates the understanding of how our systems will operate in different conditions and helps us make predictions about how system responses will respond to changes in their environment or input parameters. The process of quantifying the uncertainties in the outputs resulting from uncertain inputs is also referred as uncertainty propagation (UP).

4.2 Uncertainty Quantification Methods

There are several methods using for quantifying uncertainties, including probabilistic and non-probabilistic approaches as shown in Figure 4.1. While simulation based methods, local expansion based and functional expansion based methods, numerical integration based methods, surrogate based methods, and most probable point based methods can be given as examples to the probabilistic approaches; interval analysis, Fuzzy theory, possibility theory, and evidence theory are the most common non-probabilistic approaches.

4.2.1 Probabilistic methods

4.2.1.1 Simulation based methods

Although analytical methods are more computationally efficient and usually provide accurate results, they cannot consider the intricate structural and functional characteristics of complex systems, and this leads specialists to make unrealistic assumptions in order to achieve a certain level of accuracy [57]. In contrast, simulation-based methods, such as Monte Carlo Simulation (MCS) [58]–[61], Importance-Sampling [62,63] and Adaptive-Sampling [64] Methods are ideal for evaluating the reliability and performance of multi-state systems, as they replicate the actual system operation. However, these methods require significant computational

resources and are typically customized for a specific system. Simulation-based methods can handle any transition distribution, enable the examination of the impact of external factors on system performance [60], and can be seamlessly combined with other methods [65].

4.2.1.2 Local expansion based methods

Local expansion based methods such as Taylor series and perturbation methods [66,67] are generally utilized for scenarios with limited variations in input and outputs that exhibit minimal nonlinearity.

4.2.1.3 Function expansion based methods

Functional expansion based methods contains to a variety of techniques such as Neumann expansion, Karhunen–Loeve expansions (KLE) [68], Polynomial Chaos Expansion (PCE) [69]–[72]. Among this methods, PCE is the most common one and it has received increasing attention in recent years [73]. PCE method is a non-intrusive spectral stochastic method allows for the efficient propagation of uncertainty through mathematical models by representing the input uncertainties as random variables with known probability distributions and then approximating the output of the model as a polynomial in terms of these random variables. The coefficients of the polynomial are obtained using statistical moments of the input random variables, such as the mean and variance, and the method can be used to estimate the statistics of the model output, such as the mean, variance, and higher-order moments.

4.2.1.4 Most-Propable-Point based methods

Most-Probable-Point (MPP) based methods are the methods offer the advantage of striking a balance between computational efficiency and accuracy [74]. The First-Order Reliability Method (FORM) [75] and the Second-Order Reliability Method (SORM) [76] can be said the the most widely used Most Probable Point based techniques.

4.2.1.5 Numerical integration based methods

Numerical integration based methods [77,78] first use direct numerical integration to calculate statistical moments. Then, they approximate either the probability density or the tail region probability using empirical distribution systems that rely on the calculated moments. The Full Factorial Numerical Integration (FFNI) method [78,79] computes the statistical moments of the performance function by directly integrating it using a suitable quadrature formula while Dimension Reduction (DR) method [79]–[81] involves approximating a complex integral involving multiple dimensions by breaking it down into simpler integrals with fewer dimensions, and this is achieved through the use of an additive decomposition technique applied to the performance function [73].

4.2.1.6 Surrogate based methods

The surrogate modeling method is a cost-effective and rapid technique for mapping responses, also known as a meta-model, that serves as a replacement for running a simulation [82]. This approach is typically favored when the expense of sampling or computation is high for complex simulations. Many surrogate methods are available, including the Kriging (also known as Gaussian Process) method [83], which has the capability to interpolate predicted data and provide statistical information at unsampled locations in the parameter space, and the Radial Basis Function (RBF) [84] method, which can accurately interpolate sample points and provide either locally or globally interpolated values depending on the chosen radial basis function [57]. Surrogate modeling process and some of the surrogate methods are also discussed in Section 5.2.

4.2.2 Non-Probabilistic methods

Non-probabilistic UQ (uncertainty quantification) methods such as interval analysis, Fuzzy theory, possibility theory and evidence theory refer to approaches that do not involve explicitly defining probability distributions for the input parameters. These methods rely on assumptions about the uncertainty in the input data, such as bounding the uncertainty with upper and lower bounds or assuming that the input values are

uniformly distributed within a specified range. Non-probabilistic UQ methods are often used when probability distributions for the input data are unknown, difficult to obtain, or unnecessary for the specific application.

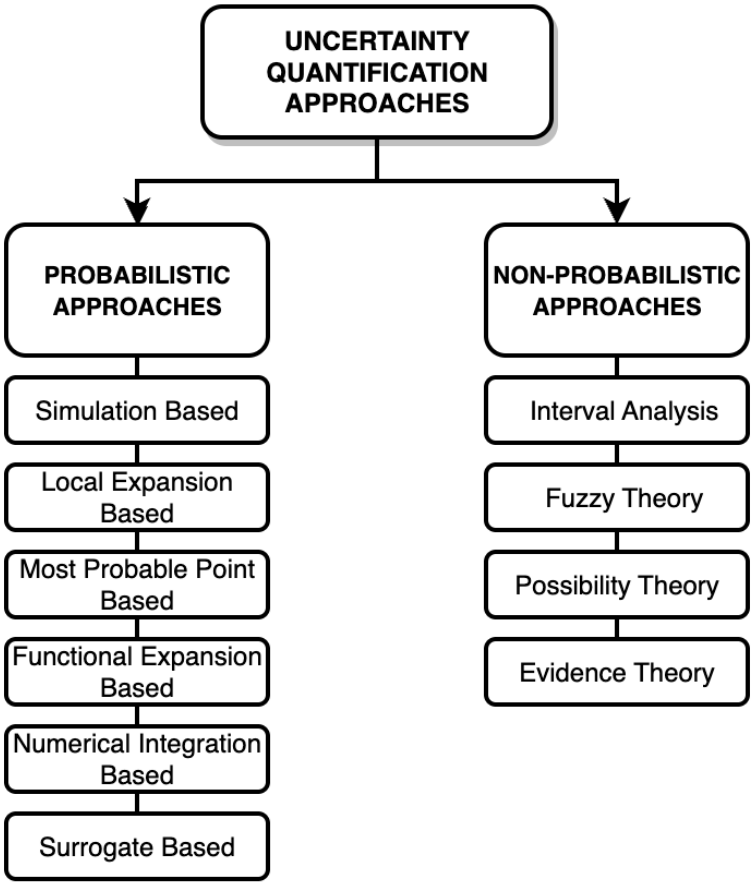

Figure 4.1 : Uncertainty Quantification Approaches.

5. METHODOLOGY

5.1 Design of Experiments (DoE)

Design of Experiment (DoE) refers to statistical approaches used to sample a function, be it a set of CFD solutions or an explicit mathematical function, in a methodical and efficient manner [85]. Many categories of such approaches exist, including Monte Carlo Sampling [86,87], Quasi-Monte Carlo Sampling [87,88], Latin Hypercube Sampling (LHS) [88]–[91], and Hammersley Sequence Sampling (HSS) [92,93].

In this study, Latin Hybercube Sampling (LHS) is selected as the DoE for the surrogate model, because of its capability to providing more accurate mean values of the function than monte Carlo sampling [9]. Sampling model and the distribution of the input parameters used in this study is shown in Figure 5.1. *x* and *y* values represent the angle of attack (α) and cavitation number (σ) parameters, respectively.

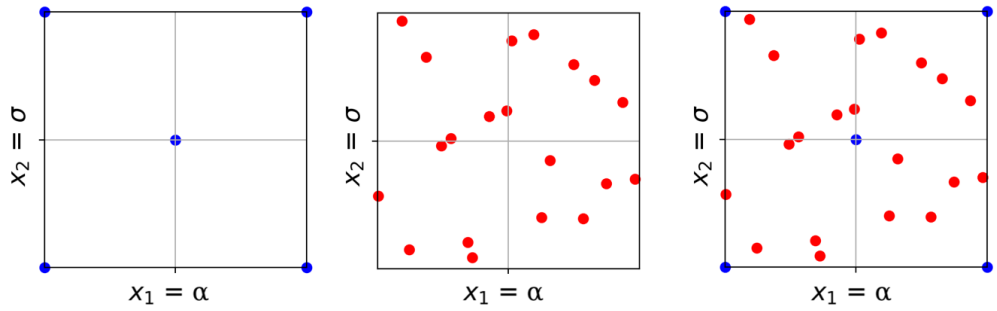

Figure 5.1 : Sampling created for two uncertain input parameters which are (α) and (σ), by applying Shell distribution (left); Latin Hybercube Sampling distribution (center), and combined LHS + Shell distribution (right).

Overall 25 sample points, which are randomly 20 sample points and 5 points which 4 are in the corners of the domain and 1 is in the center of the domain, are distributed along the domain using a combination of shell distribution and LHS distribution.

Leroux [8] studied with NACA66 foil which has identical dimensions of this study, and analyzed, observed and also photographed the partial cavitation growth and/destabilization cycles for 6 degrees attack angle and 7 different sigma values.

Angle of attack and one of the sigma values in Leroux's study are chosen to create the distribution (sigma = 1.3794). Then 5% less and more than the selected values are chosen as our range limits for sampling. According to cfd results conducted with the first sampling, it is observed that some cases -because they are very close to the unstable partial cavitation region- exhibit unstable properties (an unstable structure, especially in cavitation size and volume, since periodic sheet cavity occurs). Therefore, for a more stable cavitation to occur, a different validation data (σ = 1.5494) in Leroux's study, is accepted as the new cavitation number. Then, by repeating the previous process, $\pm$ 5% of the sigma value is determined as the sampling limits. The old and new sample spaces and the cavitation behaviors created with old and new sigma values are shown in Figure 5.2.

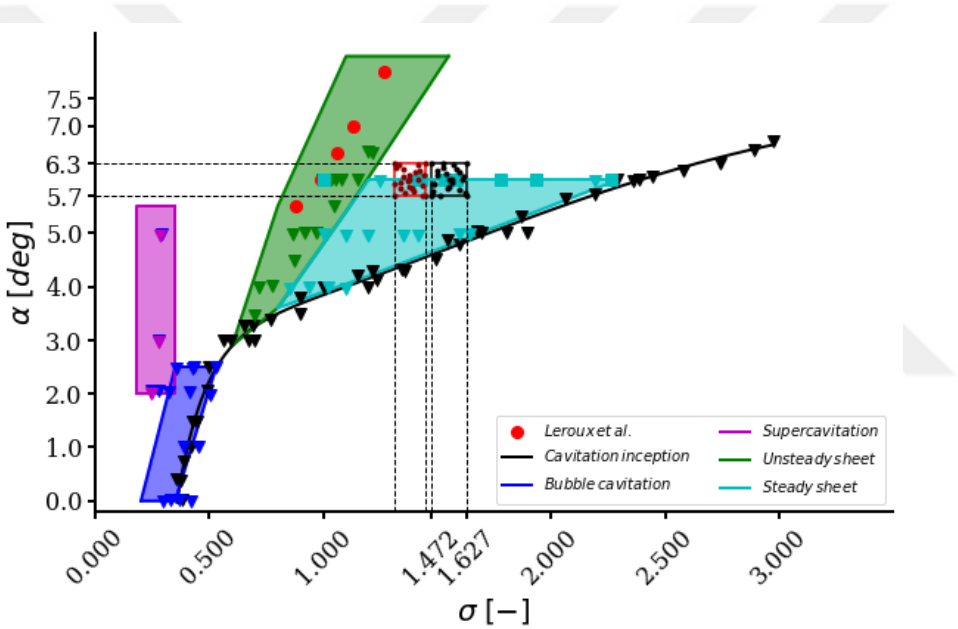

Figure 5.2 : The red rectangle and the red dots inside represent the old sampling (left), the black rectangle and the black dots inside represent the new sampling (right).

5.2 Surrogate Modeling

A surrogate model (also called as meta-model or response surface approximation) is a function which approximates the results of an an experiment or a simulation and is computationally less expensive than approach originally used to produce the data. In this approach, instead of sampling the large number of samples needed for UQ analysis, a suitable surface is defined with the data generated with a smaller number of samples. Then, the values of the desired points on the surface can be obtained by using

the response surface equation. Sobester et al. [94] outlines the modeling steps that need to be followed in order to create a surrogate model. These are arranging the data and selecting an approach for modeling, forecasting and running of the parameters, and testing the model. Different types of surrogate model approaches such as Polynomial Chaos Expansios (PCE) [95]–[97], Kriging model (also known as a Gaussian process model) [98]–[100], Multivariate Adaptive Regression Splines (MARS) [101]–[104], Radial Basis Functions (RBF) [98,105,106], Artificial Neural Networks (ANN) [98,99,107], Moving Least Squares (MLS) [108]–[110], and multifidelity models [98,111] are discussed and compared in many studies in various fields. However, the mentioned methods indirectly require that the related output parameters have to vary smoothly according to uncertain input parameters. In cases where the output parameters are not properly distributed according to the input parameters, that is, a smooth response surface is not guaranteed, these methods may significantly reduce the accuracy. Some studies have also been carried out to develop techniques for such non-smooth responses. Zhang et al. [112] developed the Adaptive Hybrid Functions (AHF) which is a new high accuracy hybrid surrogate modeling technique that combines the favorable characteristics of several surrogate models in order to model non-smooth functions. Methods are presented by Shimoyamaet al. [113] in order to obtain the polynomial chaos coefficients for modeling the non-smooth responses. A method involving two stages where the behaviors that are unique are initially identified and classified and thereafter approximations made locally is studied by Moustapha et al. [114] for non-smooth functions encountered in engineering problems. Similar studies for non-smooth response functions have been investigated in [115]–[117]. In this study involving a steady-sheet cavity flow, it is expected that to have simple, smooth response surfaces to be formed for the desired output parameters (lift coefficient C_L, drag coefficient C_D, cavitation length V_{cav}, and cavity volume V_{cav}) according to the determined inputs (angle of attack α, and cavitation number σ) will be smooth. Hence, the approach suggested by Sakata (2014), which involves utilizing a surrogate model based on a piecewise linear approximation, is employed. Linear interpolations are carried out between the three closest sampling points in this method. Being more consistent due to their lower-order nature compared to polynomial-based

approximations, is the advantage that makes this approach stand out. The utilization of the piecewise linear method in numerous applications is illustrated in [117], which provides a comprehensive overview of this approach. An example response surface and the surrogate model created according to the input parameters distribution and their response outputs $z = f(x,y)$ calculated from the CFD simulations is shown in Figure 5.3.

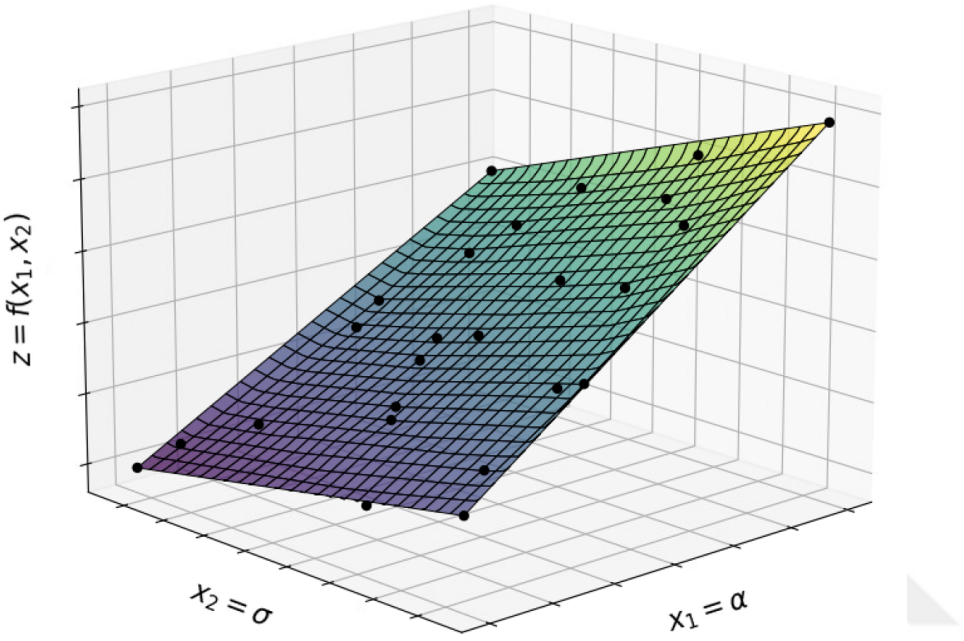

Figure 5.3 : Surrogate model for the drag coefficient (C_D): Actual response and sampling points (indicated by black dots) taken from the CFD results.

5.3 Global Sensitivity Analysis and the Sobol Method

In global sensitivity analysis, unique parameter pairs are created by assigning different values to the input parameters in the system simultaneously within a certain domain. Thus, it is possible to see the relative effects of the input parameters on the output parameters, the interactions of the input parameters, as well as the effects of these interactions on the results. In summary, sensitivity analysis is an approach used to determine how much influence a given input parameter has on the behavior of the system, or which parameters interact with each other and how much this interaction affects the results [118].

Sobol [119] introduced an approach that would later be referred to as the Sobol's method which makes it possible to compute the total contribution of each individual input parameters and their interactions to the output's variance [118,120]. In the Sobol's method, it is aimed to determine how much of the change in the output parameters of the model is either due to the change of a single parameter individually or the interaction between different input parameters. The selection of the input parameters and the reasons for the change are not emphasized, only the extent to which the changes of the input parameters have an effect on the output parameters. The flow chart and the steps of the Sobol sensitivity analysis are given in Figure 5.4. The complete process consists of the preparation step to the Sobol analysis, referred to as pre-Sobol analysis, and the main Sobol sensitivity analysis step. Sobol sensitivity analysis can be applied by following four steps which are generating the parameter sets, running the simulations for generated input parameter combinations and obtaining the model output data, calculating the Sobol indices, and analyzing the total, first, second and higher-order Sobol sensitivity indices [118].

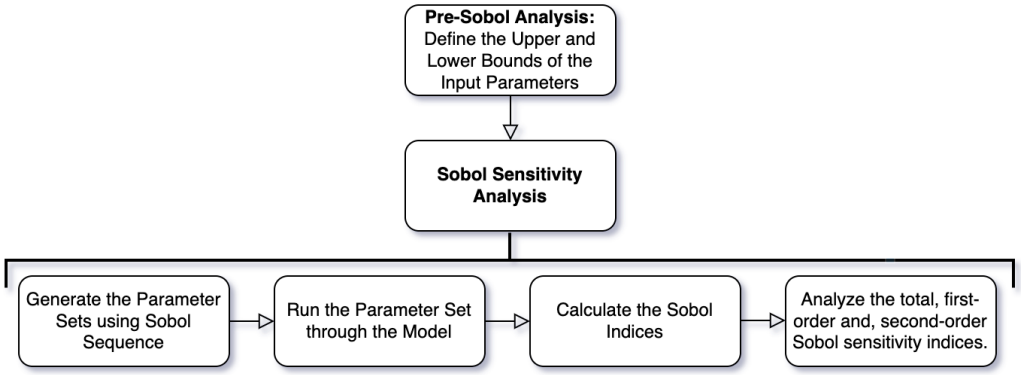

Figure 5.4 : The flow chart and the steps of the Sobol sensitivity analysis.

Consider $\mathbf{X} = (X_1, X_2, ..., X_N)$ as the input parameters and $Y = f(X_1, X_2, ..., X_N)$, as an output of the model, in which N represents the number of inputs. Indices which measure the contribution of the uncertain input parameters individually to the output Y are the first-order Sobol indices (S_i), defined as:

$$S_i = \frac{V_{X_i}\left(E_{\mathbf{X}_{\sim i}}(Y|X_i)\right)}{V(Y)} \tag{5.1}$$

where $V(Y)$ indicates the variance of Y and $E_{\mathbf{X}_{\sim i}}$ the expectation taken over all X in $\mathbf{X}$, except X_i. S_i is a number between 0 and 1 where a high value indicates an important

variable. Higher order indices, e.g. second-order (S_{i+j}), measure the contribution of the interaction between the inputs, which results in:

$$\sum_{i=1}^{N} S_i + \sum_{1 \leq i \leq j}^{N} S_{i+j} + ... + S_{i+j+k...+N} = 1 \tag{5.2}$$

For three input parameters, as we are considering in this study, this leads to:

$$S_1 + S_2 + S_3 + S_{1+2} + S_{1+3} + S_{2+3} + S_{1+2+3} = 1 \tag{5.3}$$

Total-order index (ST) considers the contribution of all the first- and high-order indices and sum of all ST equals to 1 [121]–[123], defined as:

$$ST_i = \frac{E_{\mathbf{X}_{\sim i}}(V_{X_i}(Y|\mathbf{X}_{\sim i}))}{V(Y)} \tag{5.4}$$

which leads to the following total-order indices for three input parameters to:

$$\begin{aligned} ST_1 &= S_1 + S_{1+2} + S_{1+3} + S_{1+2+3} \\ ST_2 &= S_2 + S_{1+2} + S_{2+3} + S_{1+2+3} \\ ST_3 &= S_3 + S_{1+3} + S_{2+3} + S_{1+2+3} \end{aligned} \tag{5.5}$$

More information about the Sobol method and Sobol indices is given in [123,124]. In the context of this study, the Sobol analysis is carried out by using the Sensitivity Analysis Library (SALib) implemented in Python [125].

5.4 Output Variables And Their Statistics

An empirical probability distribution (EDF or also called Empirical Cumulative Distribution Function, ECDF) is used when the data sample cannot be fitted to any known probability distribution function or cannot be obtained by data transformations or parameterization of the distribution function. To put it differently, the empirical cumulative distribution function is created based on observed data, as opposed to the cumulative distribution function which is a theoretical concept. In this study, EDFs are evaluated from the input parameter distribution in order to estimate the CDFs of the output variables. Given N_i samples x_i, the EDF for the value t is numerically calculated

by:

$$EDF(t) = \frac{1}{N_i} \sum_{n=1}^{N_i} H(t - x_i[n]) \rightarrow CDF(t) \tag{5.6}$$

where $H(x)$ is the Heaviside function. The empirical CDF usually approximates the CDF quite well, especially for large samples. If the number of samples N_i tends to infinity, EDF converges to the CDF for every value of t [126]. Considering p and $\bar{p}$ to be two probability levels, the confidence interval between them can be calculated by taking the inverse of the cumulative distribution functions (also known as the quantile function). Here, confidence level is taken to be 95% as it is generally adopted in the literature [9]. A more stringent criterion could be selected in safety-critical applications, for instance. The length of the error bars is calculated as:

$$CI_{length} = CDF^{-1}(0.975) - CDF^{-1}(0.025). \tag{5.7}$$

5.5 Combined Grid and Parameter Uncertainty

Combination of parameter and discretization uncertainty processes is carried out by applying the method proposed by Katsuno et. al. [9]. In this context, uncertainty due to discretization is included in the Sobol analysis as an extra input variable. This value is denoted as x_{grid} and refers to the point on the distribution representing the discretization uncertainty's percentile. Simulations of the 25 selected conditions are run for each grid refinement level and response surfaces are obtained for each grid. This is illustrated in Figure 5.5.

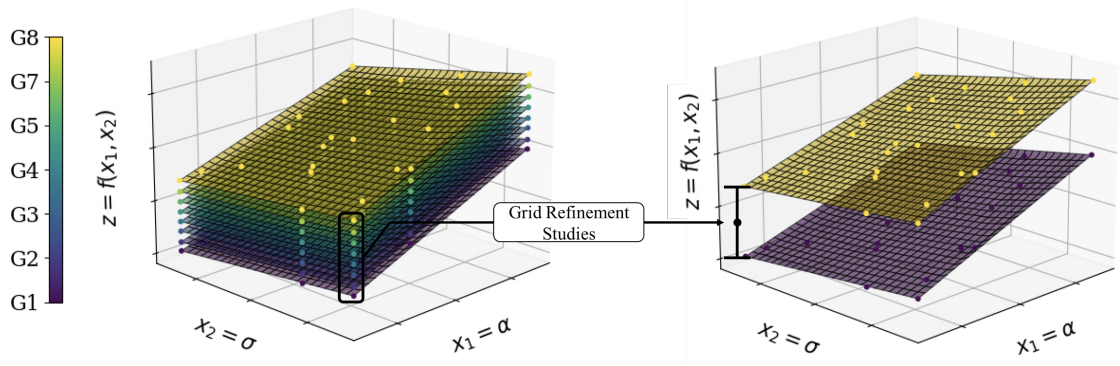

Figure 5.5 : Surrogate models for each grid refinement levels. G1 represents the coarsest grid, G8 represents the finest grid. Response surfaces are created on each grid first and then combined in the final part of the analysis.

There are 8 surrogate models for the 8 different meshes (G1 is the coarsest grid and G8 is the finest grid), each of them created by the results of CFD simulations. For an input parameter couple (x_1, x_2), there are 8 different output parameter values of $z = z(x_1, x_2)$. These are used in the numerical uncertainty estimation method of Eca and Hoekstra [127], which yields a least-squares fit to the simulated data as a function of grid refinement level, as well as the confidence interval.

After discretization uncertainty x_{grid} is defined as the third input uncertainty, the probability density function of it is defined. Due to its definition, the PDF of x_{grid} is always non-negative and its integral over the entire space is equal to one. These definitions are given in Eqs. (5.8a) and (5.8b), assuming the discretization PDF is presented as h(x).

$$h(x) \geq 0 \tag{5.8a}$$

$$\int_{-\infty}^{+\infty} h(x)dx = 1 \tag{5.8b}$$

$$\int_{y_b}^{y_t} h(x)dx = 0.95 \tag{5.8c}$$

$$\int_{-\infty}^{\phi_1} h(x)dx = \int_{\phi_1}^{+\infty} h(x)dx = 0.5 \tag{5.8d}$$

$$\int_{-\infty}^{+\infty} x.h(x)dx = \phi_0 \tag{5.8e}$$

Representing the value obtained from the finest grid by ϕ_1, the confidence interval (CI) of the numerical uncertainty evaluation process is 95% between the bounds $y_b = \phi_1 - u$ and $y_t = \phi_1 + u$. The bounds are in equal distance from the ϕ_1 and, ϕ_1 represents the median point which means the probability of getting a higher or lower value from the median value is equal, as expressed in eqs. (5.8c) and (5.8d), respectively. In similar mesh refinement applications in CFD, generally it is seen that the output response tending to increase or decrease as the grid is refined. The trend of the Richardson extrapolation function can be used to monitor this tendency. If the function displays a concave behavior, it suggests that the output response will decrease as the mesh is refined. Conversely, if the function shows a convex behavior, then the output is expected to increase as the mesh is refined. It is desired to have a PDF which behaves like the convexity of Richardson extrapolation. Because of that, the expected value of the discrezation uncertainty h(x) is assumed as ϕ_0 in the last hypothesis adopted. This

is not the exact usage of ϕ_0, its actual representation is to the idea of having a infinite mesh, but here it is used to state which value should be expected. All the assumptions are given below. Further explanation is given by [9].

6. TEST CASE

In order to investigate the combined uncertainty in the estimation of dynamic cavitation inception, NACA 66 foil which is studied experimentally by [8] and other authors, is chosen due to its popularity and its affinity to marine propeller design, and wide availability of experimental and reference numerical data [128]–[134].

6.1 Geometry

A two-dimensional cambered foil of the NACA 66 series, has relative maximum thickness of 12% at the chordwise ordinate x/c=0.45 from the leading edge. The relative maximum camber is 2% and is located at x/c=0.50 from the leading edge. The chord length c is 0.150 m. The flow is considered to be two-dimensional. Further description of the experimental set up is given in [8].

6.2 Computational Domain, Initial and Boundary Conditions

The process of determine to the dimensions of the computational domain, initial physics conditions, and boundary conditions take a crucial place in CFD simulations because they have significant effects on the behaviour of the flow. The geometry of the domain and the boundary conditions of this study are shown in Figure 6.1. A rectangular domain is used for the simulation in order to mimic the test section of the cavitation tunnel used in the source experimental study. The domain extends 0.4125 m upstream and 1.050 m downstream directions. Velocity inlet boundary condition is used at the inlet and fixed pressure is prescribed at the outlet of the domain. Symmetry boundary conditions are selected for the top and the bottom parts of the domain and a no-slip wall boundary condition is assigned to the hydrofoil. Inflow velocity is given as 5.33 m/s, leading to the same Reynolds number as in the reference experimental study [8].

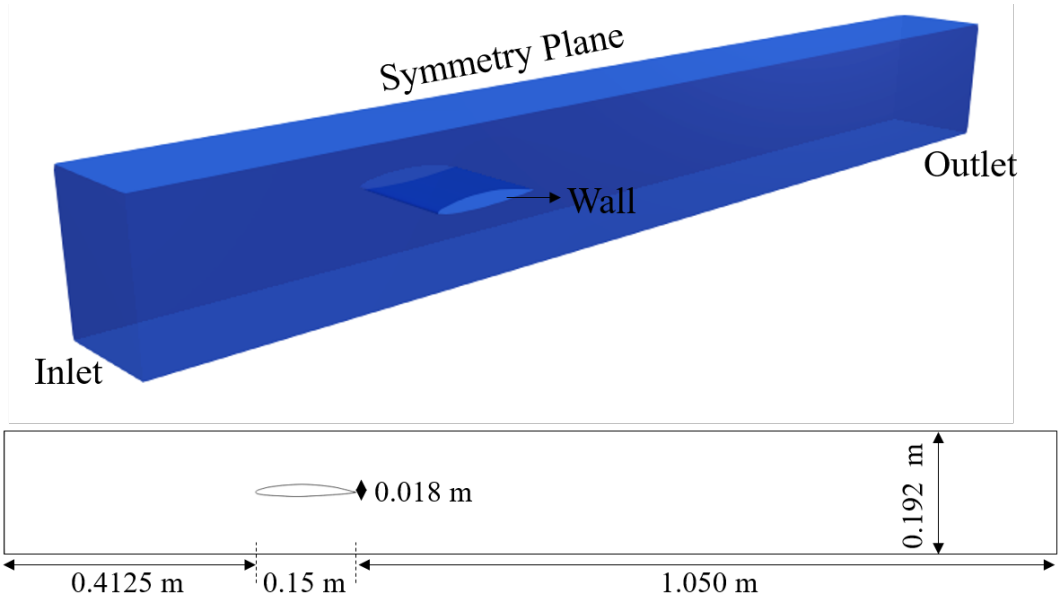

Figure 6.1 : Domain geometry and boundary conditions.

6.3 Grid Topology

The symbol "h" denotes the typical cell size, which is calculated as $1/\sqrt[3]{N}$, where "N" refers to the total number of cells. As a result, the relative increment in step size between the coarser grids, indexed by "$i \geq 1$", and the finest grid with "$i = 1$" is becomes

$$\frac{h_i}{h_1} = \sqrt[2]{N_1/N_i}. \tag{6.1}$$

Mesh G1 (the coarsest mesh, out of eight refined meshes studied in the framework of this study) topology along the whole computational domain and different section views of leading edge area from other refined grids are shown in Figure 6.2 Also, names and the characteristics of the grids are given in Table 6.1.

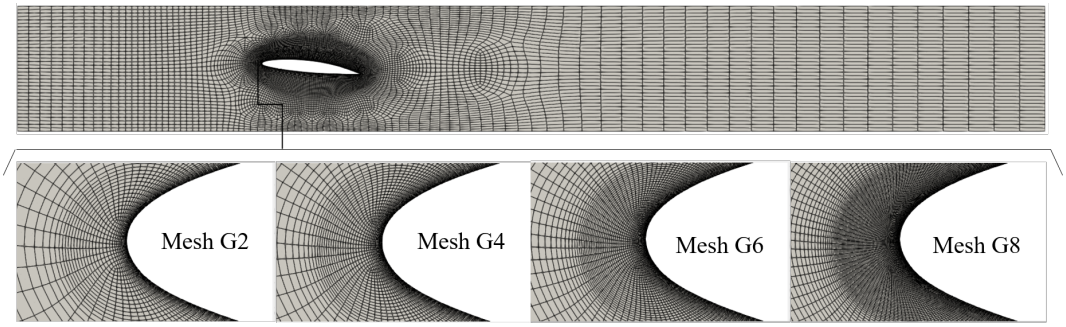

Figure 6.2 : View of the grid G1 topology of complete computational domain (top); and views of leading edge area from different refined grids (bottom).

Table 6.1 : Characteristics of the grid series used in the present study.

Mesh Name	Refinement Ratio (f)	Cell Count	Relative step size (h_i/h_1)
G1	0.7	45,184	2.4434
G2	0.8	55,476	2.2447
G3	0.9	79,156	1.9459
G4	1.0	91,632	1.7389
G5	1.2	136,620	1.4241
G6	1.4	171,088	1.3236
G7	1.6	227,680	1.1081
G8	1.8	269,808	1.0000

6.4 Numerical Setup

Simulations are carried out by using the multi-phase viscous flow solver ReFRESCO version 2023.1.0. The code was first developed within the VIRTUE EU Project [135] and is still being developed by specialists of MARIN and multiple participants all around the world.

Because of the need to achieve tight iterative convergence tolerances in order to facilitate accurate uncertainty quantification, careful choices of the discretisation schemes and solver settings are made. The momentum conservation equations are solved by using PETSc-GMRES solver with JACOBI preconditioner and discretised using the LIMITED QUICK scheme for the convective flux discretisation. For pressure equation, PETSc-CG solver with BJACOBI preconditioner is used. Turbulence is modelled by using Scale-Adaptive-Simulation Model (KSKL-Standard) turbulence model and turbulent transport equations are solved by PETSc-GMRES solver with BJACOBI preconditioner. Cavitation modeling is carried out by using Schnerr-Sauer cavitation model [136].

At the beginning of the simulation, the initial pressure is given as -250 kPa in order to prevent the presence of cavitation. After the steady non-cavitating flow has been established, the saturated vapour pressure value is gradually adjusted following a Hermite polynomial to reach to the desired cavitation number. Foil angle of attack obtained by deforming the baseline grid that has been generated at a zero incidence angle. In this approach, the cells in direct vicinity to the foil surface are fixed to the solid body and those further away are deformed using radial basis functions. This

approach avoids the need to generate a new grid for each condition, speeding up the computations and ensuring that the results remain consistent within the complete matrix of simulations. Residual convergence criteria are set to $1x10^{-5}$ in L_∞ norm for all transport equations. Additional key parameters of simulation setup are listed in Table 6.2.

Table 6.2 : Key parameters of simulation setup.

Parameter	**Value**	**Unit**
Dynamic viscosity, μ	$9.9938x10^{-4}$	kg (m s)$^{-1}$
Water density, ρ_w	1000	kg m^{-3}
Inflow speed, U_∞	5.33	m s $^{-1}$
Reynolds number, Re	8 x 10^{-4}	-
Cavitation number, σ	1.3105 to 1.4484	-
Angle of attack, α	5.70 to 6.30	deg
Vapour density, ρ_v	0.024	kg^2 m^{-3}
Bubble kinematic viscosity, ν_B	$1.02 \cdot 10^{-5}$	m^{2}s^{-1}

6.5 Input and Output Variables

Angle of attack (Aoa) is the angle between the chord line and the relative flow direction. Increase in attack angle also increase both lift and drag forces up to the stall angle. Cavitation number is a non-dimensional parameter describing how prone to cavitation a particular flow is. It is calculated by using a reference pressure (p), saturated vapor pressure (p_v), density of fluid, and velocity of flow:

$$\sigma = \frac{p - p_v}{\frac{1}{2}\rho_w U_\infty^2}. \tag{6.2}$$

The lower the cavitation number, the higher the probability of cavitation. In this study, velocity of the flow, density and reference pressure are kept as constant. Saturation pressure values in each case is changed to achieve the desired cavitation number.

Lift Coefficient is a non-dimensional quantity that gives the relation of the lift force generated by a lifting surface to the density of fluid, flow velocity and the reference area. In this study, the lift force is considered as the force generated by the foil in the positive y-direction (F_Y) and is calculated as

$$C_L = \frac{F_Y}{0.5\rho U_\infty^2 cs}. \tag{6.3}$$

The drag coefficient is non-dimensional quantity employed in fluid dynamics to assess the resistance or drag produced by an object in a fluid medium. In this study, drag force is considered as the force generated by the foil in the x-direction (F_X). It is computed according to

$$C_D = \frac{F_X}{0.5\rho U_\infty^2 cs}. \tag{6.4}$$

Cavitation length is computed by finding the minimum and maximum extents of the stable sheet cavity present on the hydrofoil. In order to make the results more consistent and representative of what would be observed visually during the experiments, only cells with vapour volume fraction higher than 0.25 are taken into account in the computation. The obtained value is then non-dimensionalised by the chord length, leading to

$$L_{cav} = \frac{x_{cav\,max} - x_{cav\,min}}{c}. \tag{6.5}$$

Total cavitation volume is obtained by performing a finite weighted sum of all the cells filled with vapour. The final result is made non-dimensional by using the span length and square of the chord length, or

$$V_{cav} = \frac{\sum_{iCell=0}^{N_{cells}} V_{iCell}\,\alpha_{iCell}}{sc^2}. \tag{6.6}$$

7. RESULTS AND DISCUSSION

In the first stage of this study, CFD simulations with and without cavitation were made in order to compare the results with the experimental results given in the study of Leroux et al. [8].

Interestingly, for high cavitation numbers, corresponding to little cavitation, the most pronounced differences may be seen. This is likely indicative of discrepancies between the numerical and experimental set ups that cannot be accurately discerned from the description of the experiments provided in [8] and [137]. At the same time, the trends in the analysed quantities, especially drag and cavity length, match the experiments very well. The magnitude of the lift coefficient also matches the measurements more closely at low σ values with a relative error of under 3%.

Iterative convergence of the SIMPLE algorithm inside each CFD time step is necessary for UQ applications in CFD in order to guarantee that true sensitivities and not numerical noise are being analysed inside the batch of simulations used as UQ inputs. One of the most influential parameters in achieving good iterative convergence is the Courant number. Due to use of an implicit time scheme, having a maximum Courant number approximately 10 has been found to be acceptable. Usually, approximately 80 outer loops were performed within each time step with a hard maximum of 100 imposed in order to reduce the risk of the simulation getting stuck at a time step that is particularly difficult to converge. The residuals for a case of intermediate refined mesh (G4) is shown in Figure 7.1. Two normalization types which are L_2 and L_∞ are chosen to check convergence of the simulations. As can be seen, after approximately 3000 time steps, corresponding to the establishing of a fully-developed flow, the residuals converge in a repetitive fashion.

Although the chosen experimental condition may be classified as steady sheet cavitation, in reality small oscillations of the trailing edge of the cavity were observed in the computations. In order to guarantee statistical convergence of the results,

25,000 time steps were used in each computation, with the first 1,000 time steps being discarded from the analysis due to start up effects. Time histories of the considered output quantities obtained from an example simulation are depicted in Figure 7.2.

A python module called pyTST which implements the "Transient Scanning Technique" presented in [138]–[140] is used to check whether the selected number of time step is sufficient or not. pyTST module allows to detect transient portion of a signal and measure the statistical uncertainty with that portion removed [141].

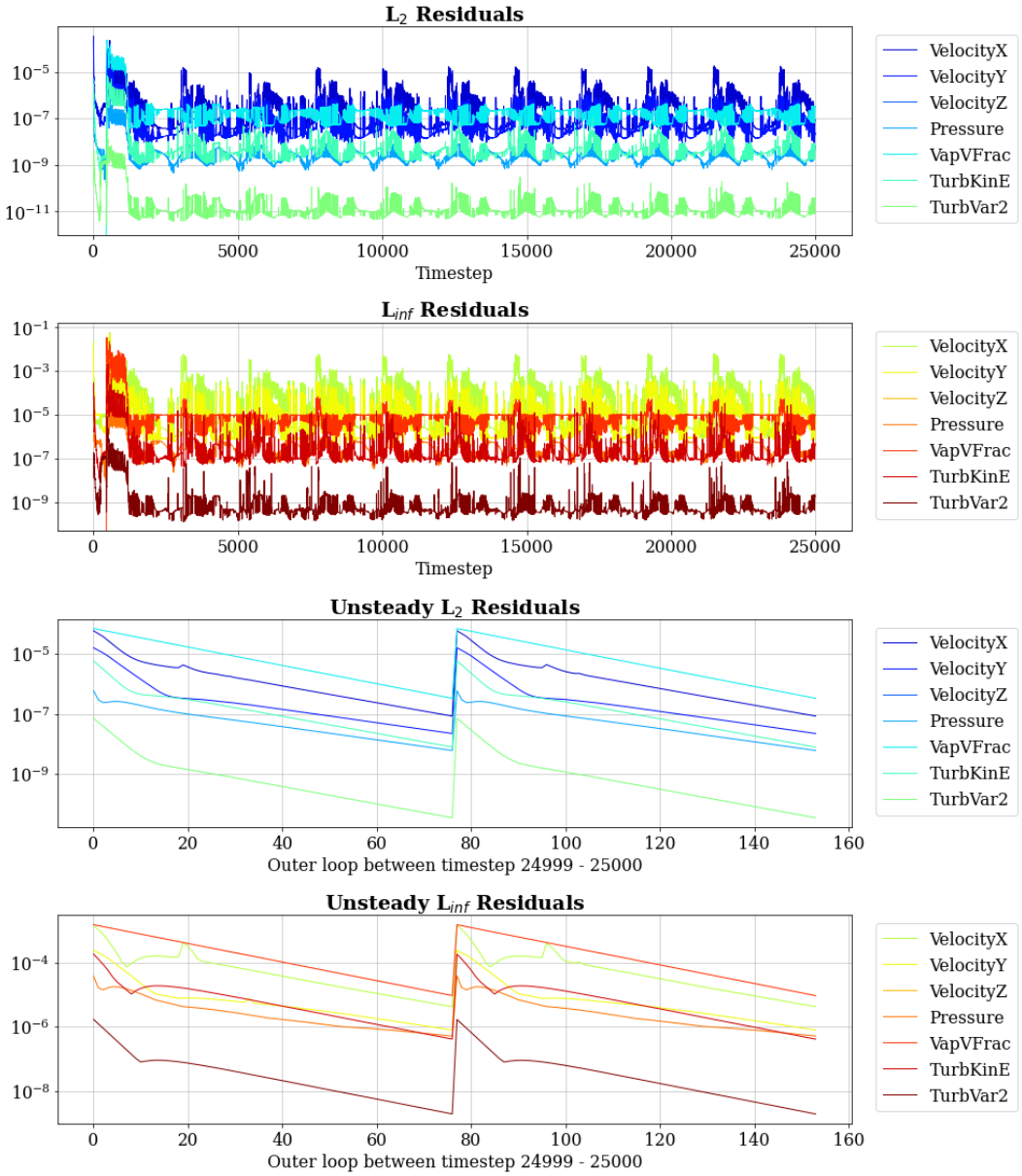

Figure 7.1 : L_2 and L_∞ residuals of a case for intermediate refined mesh (G4) for input parameters as $\sigma = 1.6102$ and $\alpha = 6.0065°$.

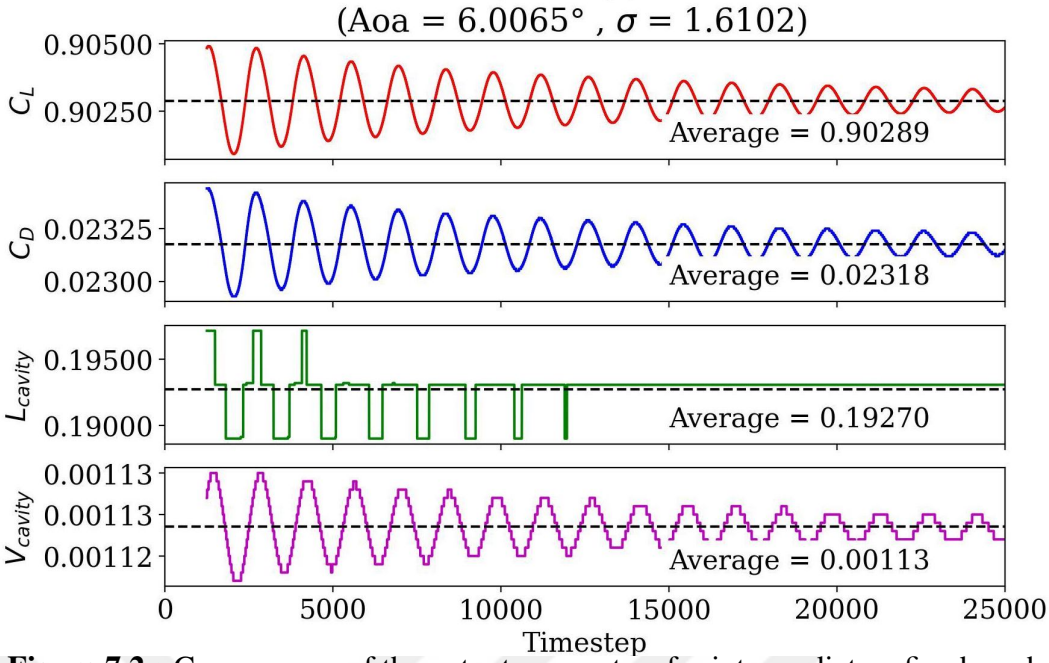

Figure 7.2 : Convergence of the output parameters for intermediate refined mesh (G4) for input parameters as $\sigma = 1.6102$ and $\alpha = 6.0065°$.

Quantification of uncertainties was carried out across 8 grids with different densities, employing 25 sampling points. A good sampling strategy should ensure that the entire input space is adequately sampled while avoiding excessive computational cost. In order to calculate the Sobol indices more accurately, the results were investigated for 2^{11} to 2^{16} range sampling points, and it is seen that the results remain same in 2^{15} and 2^{16}. So that, 2^{15} sampling points were obtained from the response surfaces. A representative plot is given in Figure 7.3. The primary findings of the analysis include the discretization uncertainties and Sobol indices computed for both parameter uncertainty and combined uncertainty procedures. They are shown in Figure 7.4.

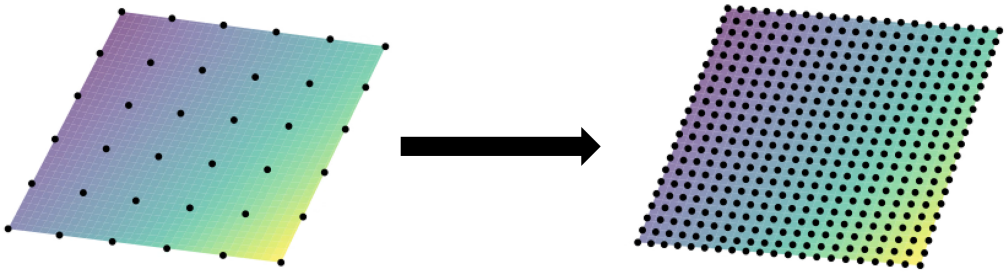

Figure 7.3 : Sampling points obtained from the response surfaces: a) 2^{10} points (Representative) b) 2^{15} points (Representative).

The h_i/h_1 values given on the x-axis indicate the relative grid size, defined as per the work of [127]. In this study, $h_i/h_1 = 1$ refers to the finest mesh and $h_i/h_1 = 2.4434$ to the coarsest mesh. The figures on the left-hand side depict discretization uncertainties, indicated by continuous error bars that rely solely on the expected values of input parameters and do not factor in parameter uncertainties. $h_i/h_1 = 0$ represents the extrapolated value corresponding to infinite grid refinement, in which case the value read on the y-axis will be the expected value of the output parameter. The error bars given for each grid show the different percentage between the value to be reached on the infinitely refined grid (expected value) and the value in that grid. The values on or below of the error bars represent the uncertainty value which is calculated by multiplying the error value with a safety factor for the corresponding grid. The expected behavior in such a plot is that the error bars get shorter as the refinement in the grid increases. Such behavior indicates that discretization-induced errors in the simulation results decrease as the grid is refined. The value in the left-below side of the figure (value on the the bottom dashed line) represent the combined uncertainty value for the corresponding output parameter. Combined uncertainty value is considers the sum of each input parameter uncertainties and discretization uncertainty. In the right-hand side figures, the colored bars represent the Sobol indices of the input parameters for each relative grid size. The bars in the left of the part of the plot correspond to the Sobol indices obtained by the combined uncertainty approach containing both the parameter and grid uncertainty. Coloured lines represents the total-order Sobol indices. Additionally, markers are used to display the total-effect Sobol indices of the combined approach.

In the two plots on the top row for the C_L parameter, the magnitude of the discretization uncertainty does not decrease further with grid refinement providing results with 0.0% - 0.1% uncertainty margin, i.e. very close to the expected value for the C_L parameter. This shows that even the coarsest grid is sufficient for the determination of this parameter. The combined uncertainty for C_L parameter is 4.70%. The greater effect on this value comes from the input parameter uncertainties, especially from the angle of attack S_α. In the combined uncertainty analysis, the individual effect of the S_α index (angle of attack) decreased from 0.99 to 0.84, while ST1, which expresses

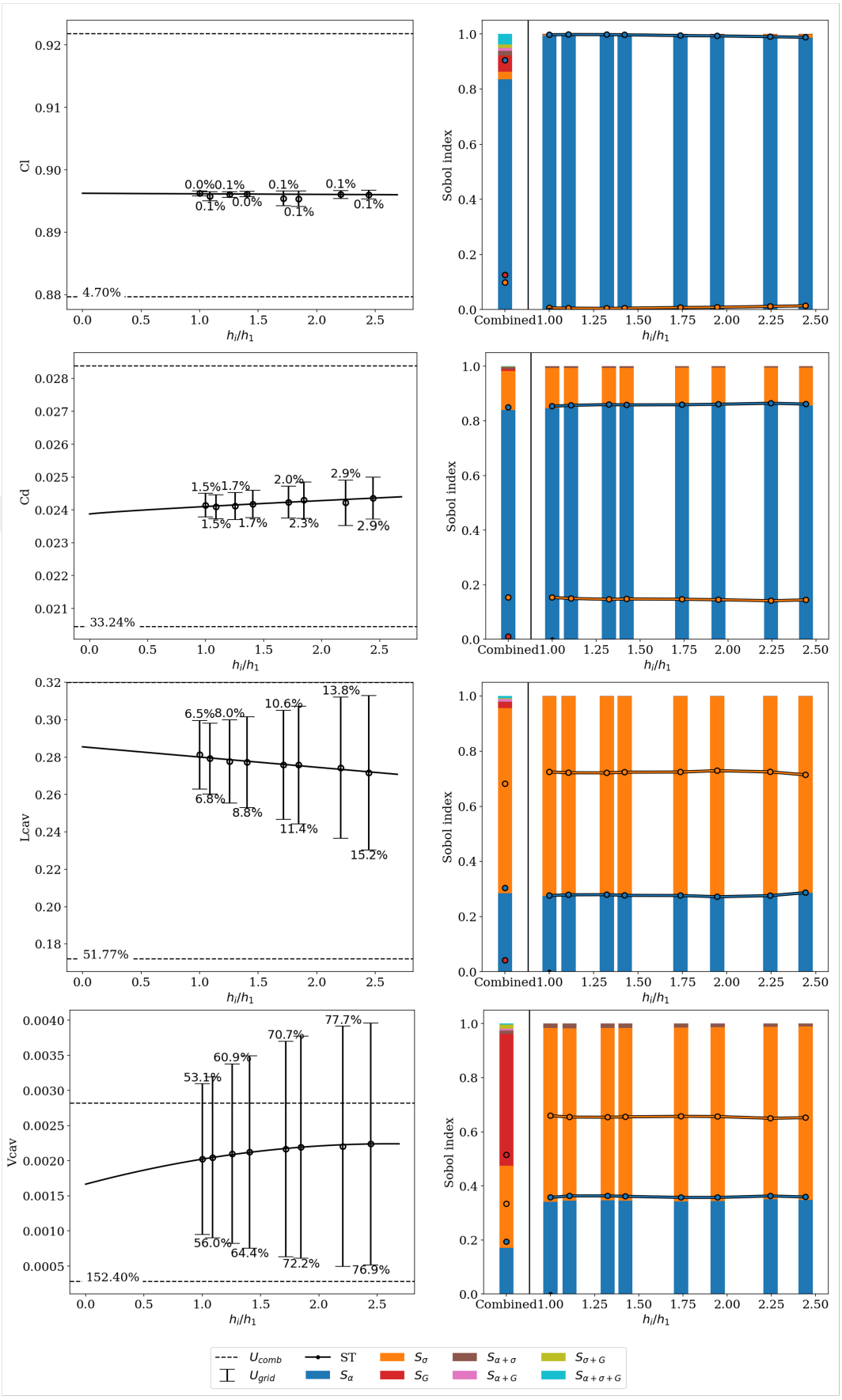

Figure 7.4 : Comparison between parameter uncertainty and discretization uncertainty U_{grid}. Sobol indices are illustrated for each grid and combined uncertainty (on the right), with total-effect Sobol indices depicted using lines.

the total effect of the first parameter including its interaction with the second and third parameters, decreased to 0.90. Also, it can be observed that the effect of the cavitation number parameter, which almost cannot be seen on parameter uncertainty bars, increases noticeably here. In addition, by looking at the red colored part of the combined uncertainty bar, namely the Sobol index (S_G) of the grid refinement parameter, it can be seen that the grid has more effect on C_L than the cavitation number. Although refinement ratio did not affect the accuracy of the results much (according to the grid-uncertainty bars of C_L), it is seen that it the changes the influence of input parameters on the results.

Looking at the left-hand side figure for the C_D parameter, it is seen that in the discretization uncertainty study, the four coarsest grids have a 2.9% uncertainty according to the expected value of C_D in the infinite refinement state of the fitted exponential curve. Although this uncertainty value is higher than the uncertainty in the C_L parameter, it is deemed acceptable for practical purposes, particularly in the light of the aforementioned likely discrepancies between the numerical and experimental set ups. When the grid refinement process is continued, the uncertainty level in the finest grid decreases to 1.5%, showing that if the grid is sufficiently refined, the expected value can be approached but far more cells would be required to drive the uncertainty to a magnitude comparable to that of the lift coefficient. In the parameter uncertainty results, it is seen that the individual Sobol index of the 1st parameter (S_α - angle of attack) is dominant over the second parameter (S_σ - cavitation number), but not as dominant as in the case of C_L. Also, the effect of the first parameter, including its interaction with the second parameter (ST1), represented by the blue line, appears to be slightly different from the individual effect. The same is true for the second input parameter. This shows that the input parameters do not have a significant interaction with each other in the calculation of the C_D coefficient, and that the angle of attack of the foil is the main factor affecting the drag coefficient by itself. In the combined parameter uncertainty part, it is seen that the grid uncertainty (red) has a shorter bar than in the case of the lift coefficient. In other words, application of grid refinement does not significantly affect the results. Furthermore, the inclusion of grid uncertainty

in the analysis reduces the effect of the first input parameter on C_D, while increasing that of the second input parameter, but only slightly.

In the discretization uncertainty figure presented for the cavitation length, it is seen that the grid refinement process has more effect on the cavitation length parameter than the previous two output parameters. This inference has been made considering that the uncertainty value difference between the coarsest grid and the finest grid is around 8% for the L_{cav} value. The fact that the grid refinement process approaches the actual value of the output parameter in each refinement is exactly as expected from this process. Since the fitted exponential curve and the length of error bars decrease regularly as the relative step size (h_i/h_1) ratio decreases, it seems possible to obtain results much closer to the expected value for the L_{cav} parameter by continuing the grid refinement process. It is seen that the grid uncertainty parameter has a very low effect on the output parameters compared to the other two input parameters. This is an important takeaway, as although the grid uncertainty is quite large here (6.5%-15.2%), it is far less important than the uncertainties over the angle of attack and cavitation number.

Looking at the discretization uncertainty figure for the V_{cav} parameter, it is seen that as the grid is refined, the discretization uncertainty bars get shorter, that is, the V_{cav} value approaches the expected value. It may also be seen that the Sobol index corresponding to the discretization effect is noticeably higher for the cavitation volume than for the other output parameters. This can be understood from the fact that the uncertainty values have approximately 24% difference between the finest grid and the coarsest grid. The high levels of discretization uncertainty also indicate that further refinement would be necessary in order to arrive at a set of converged values and more reliable uncertainty estimates. In the parameter uncertainty part of the right-hand side figure for V_{cav}, it is seen that the individual effects of the input parameters are close to each other. However, as it is in L_{cav}, the cavitation number is the more influential than the angle of attack. In the combined parameter uncertainty results, it is seen that the grid uncertainty (red bar) has the greatest effect on the outputs. Also, the total-effect Sobol indices of the combined study show that the discretization uncertainty has the highest influence on V_{cav} uncertainty, with ST3 = 0.52, followed by the cavitation number with

ST2 = 0.34 and angle of attack ST1 with 0.19. To reduce the combined uncertainty, a much finer mesh is necessary.

As a summary of the results presented in this study: the discretization uncertainty may be the dominant contributor to the output uncertainties for some parameters, but the input uncertainties also have a significant and relevant effect. Furthermore, in flows where turbulence intensity is high and cavitation is present, although the selected grid can accurately capture parameters such as C_L and C_D calculated by reading the forces, it may not be as successful in capturing unstable parameters such as L_{cav} and V_{cav} . In such cases, the combined uncertainty effect would be much more. But this can be reduced by refining the grid especially for the output parameter of Vcav.

8. CONCLUSION

In this thesis study, it was demonstrated the determination of the joint impact of parameter and discretization uncertainties in CFD simulations. The results include the computation of confidence intervals and Sobol indices. Two uncertain input variables, the angle of attack and cavitation number, were chosen and evaluated on the example of a NACA66 hydrofoil. Also, in order to investigate the discretization uncertainty effect on the output parameters, grid uncertainty has been considered as the third input parameter. Although the simulations carried out were 2D, the computational cost of performing tens of computations on each grid refinement level was a significant hindrance and highlights the difficulty in applying UQ to CFD simulations. As a consequence, a surrogate model approach was employed to allow the Sobol analysis to be carried out using fewer computational results. Confidence intervals and Sobol indices for input parameters, such as drag coefficient (C_D) and cavitation length (L_{cav}), remained mostly unchanged despite variations in grid refinement. This indicates that parameter uncertainties were the dominant factor. Regarding the lift coefficient (C_L), the impact of discretization uncertainty was found to be larger than that of C_D and V_{cav}. However, it was still observed that parameter uncertainty had a more significant influence than discretization uncertainty. In contrast to other output parameters, the analysis of cavitation volume (V_{cav}) revealed that discretization uncertainty had a greater impact than parameter uncertainty. Nevertheless, the study still indicated that parameter uncertainty played a significant role in determining this output parameter.

To expand the scope of this study, future research could utilize the presented analysis framework to develop a formulation that incorporates unsteady applications and considers the impact of iterative uncertainty or time step uncertainty in addition to quantifying grid and input uncertainty. Other parameters, such as coefficients related to turbulence or cavitation models, could be included to factor in additional degrees of the modelling uncertainties in addition to the grid and operating point conditions.

REFERENCES

[1] **Brennen, C.E.** (2014). *Cavitation and bubble dynamics*, Cambridge university press.

[2] **Franc, J.P. and Michel, J.M.** (2004). *Fundamentals of Cavitation*, Springer.

[3] **Coutier-Delgosha, O. and Perrier, V.** (2005). Prediction and mitigation of propeller cavitation erosion, *Proceedings of the 16th International Symposium on Transport Phenomena (ISTP-16)*, Elsevier, pp.185–190.

[4] **Hultgren, L.S. and Jani, M.G.** (2010). Cavitation in marine propellers: A review of experimental and numerical methods, *Proceedings of the 29th Symposium on Naval Hydrodynamics*, Office of Naval Research, pp.55–67.

[5] **Arndt, R.E.A.** (1991). Propeller cavitation - An overview, *Journal of Ship Research*, *35*(3), 183–191.

[6] **Fagerström, M. and Larsson, L.** (2007). Cavitation erosion of marine propellers, *Wear*, *263*(7-12), 1138–1145.

[7] **Kim, K.W.**, **Lee, C.W. and Kang, K.Y.** (2007). Propeller cavitation evaluation using unsteady RANS analysis, *Journal of Marine Science and Technology*, *12*(2), 117–128.

[8] **Leroux, J.B.**, **Astolfi, J.A. and Billard, J.Y.** (2004). An experimental study of unsteady partial cavitation, *J. Fluids Eng.*, *126*(1), 94–101.

[9] **Katsuno, E.T.**, **Lidtke, A.K.**, **Düz, B.**, **Rijpkema, D.**, **Dantas, J.L. and Vaz, G.** (2021). Estimating parameter and discretization uncertainties using a laminar–turbulent transition model, *Computers & Fluids*, *230*, 105129.

[10] **Gindroz, B. and Billet, M.** (1998). Influence of the nuclei on the cavitation inception for different types of cavitation on ship propellers.

[11] **Mueller, A. and Kinnas, S.A.** (1999). Propeller sheet cavitation predictions using a panel method.

[12] **Iga, Y.**, **Nohmi, M.**, **Goto, A.**, **Shin, B.R. and Ikohagi, T.** (2003). Numerical study of sheet cavitation breakoff phenomenon on a cascade hydrofoil, *J. Fluids Eng.*, *125*(4), 643–651.

[13] **Kinnas, S.A.**, **Lee, H. and Young, Y.L.** (2003). Modeling of unsteady sheet cavitation on marine propeller blades, *International Journal of Rotating Machinery*, *9*(4), 263–277.

[14] **Vaz, G. and Bosschers, J.** (2006). Modelling three dimensional sheet cavitation on marine propellers using a boundary element method, *Sixth International Symposium on Cavitation CAV2006, Wageningen, The Netherlands*.

[15] **Coutier-Delgosha, O.**, **Stutz, B.**, **Vabre, A. and Legoupil, S.** (2007). Analysis of cavitating flow structure by experimental and numerical investigations, *Journal of Fluid Mechanics*, *578*, 171–222.

[16] **Foeth, E.J.**, **Van Doorne, C.**, **Van Terwisga, T. and Wieneke, B.** (2006). Time resolved PIV and flow visualization of 3D sheet cavitation, *Experiments in Fluids*, *40*, 503–513.

[17] **Szantyr, J.** (2008). The crucial contemporary problems of the computational methods for ship propulsor hydrodynamics, *Archives of Civil and Mechanical Engineering*, *8*(1), 69–95.

[18] **Arazgaldi, R.**, **Hajilouei, A. and Farhanieh, B.** (2009). Experimental and numerical investigation of marine propeller cavitation.

[19] **van Rijsbergen, M.X. and van Terwisga, T.J.** (2010). Water quality effects on sheet cavitation inception on a ship propeller model, *7th International Conference on Multiphase Flow*.

[20] **Subhas, S.**, **Saji, V.**, **Ramakrishna, S. and Das, H.** (2012). CFD analysis of a propeller flow and cavitation, *International Journal of Computer Applications*, *55*(16).

[21] **Paik, K.J.**, **Park, H.G. and Seo, J.** (2013). URANS simulations of cavitation and hull pressure fluctuation for marine propeller with hull interaction, *3nd International Symposium on Marine Propulsors, Tasmania*, pp.389–396.

[22] **Lee, K.**, **Lee, J.**, **Kim, D.**, **Kim, K. and Seong, W.** (2014). Propeller sheet cavitation noise source modeling and inversion, *Journal of Sound and Vibration*, *333*(5), 1356–1368.

[23] **Aktas, B.**, **Atlar, M.**, **Turkmen, S.**, **Shi, W.**, **Sampson, R.**, **Korkut, E. and Fitzsimmons, P.** (2016). Propeller cavitation noise investigations of a research vessel using medium size cavitation tunnel tests and full-scale trials, *Ocean engineering*, *120*, 122–135.

[24] **Helal, M.M.**, **Ahmed, T.M.**, **Banawan, A.A. and Kotb, M.A.** (2018). Numerical prediction of sheet cavitation on marine propellers using CFD simulation with transition-sensitive turbulence model, *Alexandria engineering journal*, *57*(4), 3805–3815.

[25] **Bosschers, J.** (2019). Mechanisms of low-frequency broadband noise by cavitating tip-vortices on marine propellers, *Sixth International Symposium on Marine Propulsors SMP*, volume 19.

[26] **Melissaris, T.**, **Schenke, S.**, **Bulten, N. and van Terwisga, T.J.** (2020). On the accuracy of predicting cavitation impact loads on marine propellers, *Wear*, *456*, 203393.

[27] **Herzog, M.**, **Gilg, A.**, **Paffrath, M.**, **Rentrop, P. and Wever, U.** (2008). Intrusive versus Non-Intrusive Methods for Stochastic Finite Elements, Springer Berlin Heidelberg, Berlin, Heidelberg, pp.161–174, https://doi.org/10.1007/978-3-540-74238-8_13.

[28] **Sullivan, T.J.** (2015). *Introduction to uncertainty quantification*, volume 63, Springer.

[29] **Mtre, O.**, **Knio, O.**, **Najm, H. and Ghanem, R.** (2001). A stochastic projection method for uid ow: I. basic formulation, *Journal of Computational Physics*, *173*(2).

[30] **Le Maitre, O.P.**, **Reagan, M.T.**, **Najm, H.N.**, **Ghanem, R.G. and Knio, O.M.** (2002). A Stochastic Projection Method for Fluid Flow: II. Random Process, *Journal of Computational Physics*, *181*(1), 9–44, https://www.sciencedirect.com/science/article/pii/S0021999102971044.

[31] **Xiu, D. and Karniadakis, G.E.** (2003). Modeling uncertainty in flow simulations via generalized polynomial chaos, *Journal of computational physics*, *187*(1), 137–167.

[32] **Mathelin, L.**, **Hussaini, M.Y. and Zang, T.A.** (2005). Stochastic approaches to uncertainty quantification in CFD simulations, *Numerical Algorithms*, *38*(1), 209–236.

[33] **Onorato, G.**, **Loeven, G.**, **Ghorbaniasl, G.**, **Bijl, H. and Lacor, C.** (2010). Comparison of intrusive and non-intrusive polynomial chaos methods for CFD applications in aeronautics, *V European conference on computational fluid dynamics ECCOMAS, Lisbon, Portugal*, pp.14–17.

[34] **Dinescu, C.**, **Smirnov, S.**, **Hirsch, C. and Lacor, C.** (2010). Assessment of intrusive and non-intrusive non-deterministic CFD methodologies based on polynomial chaos expansions, *International Journal of Engineering Systems Modelling and Simulation*, *2*(1-2), 87–98.

[35] **Phillips, T.S. and Roy, C.J.** (2016). A new extrapolation-based uncertainty estimator for computational fluid dynamics, *Journal of Verification, Validation and Uncertainty Quantification*, *1*(4).

[36] **Cuneo, A.**, **Traverso, A. and Shahpar, S.** (2017). Comparative analysis of methodologies for uncertainty propagation and quantification, *Turbo*

Expo: Power for Land, Sea, and Air, volume50800, American Society of Mechanical Engineers, p.V02CT47A005.

[37] **Gilli, L.**, **Lathouwers, D.**, **Kloosterman, J.**, **van der Hagen, T.**, **Koning, A. and Rochman, D.** (2013). Uncertainty quantification for criticality problems using non-intrusive and adaptive Polynomial Chaos techniques, *Annals of Nuclear Energy*, *56*, 71–80, https://www.sciencedirect.com/science/article/pii/S0306454913000261.

[38] **Carlton, J.** (2018). *Marine propellers and propulsion*, Butterworth-Heinemann.

[39] **Singhal, A.K.**, **Athavale, M.M.**, **Li, H. and Jiang, Y.** (2002). Mathematical basis and validation of the full cavitation model, *J. Fluids Eng.*, *124*(3), 617–624.

[40] **Zwart, P.J.**, **Gerber, A.G.**, **Belamri, T.** *et al.* (2004). A two-phase flow model for predicting cavitation dynamics, *Fifth international conference on multiphase flow, Yokohama, Japan*, volume152.

[41] **Schnerr, G.H. and Sauer, J.** (2001). Physical and numerical modeling of unsteady cavitation dynamics, *Fourth international conference on multiphase flow*, volume 1, ICMF New Orleans New Orleans, LO, USA.

[42] **F.R.S., L.R.O.** (1917). VIII. On the pressure developed in a liquid during the collapse of a spherical cavity, *The London, Edinburgh, and Dublin Philosophical Magazine and Journal of Science*, *34*(200), 94–98, https://doi.org/10.1080/14786440808635681.

[43] *Cavitation*, https://www.britannica.com/technology/navalarchitecture/Cavitation#/media/1/406846/147890, accessed: 2023-05-05.

[44] **Furuya, M.**, **Kajikawa, Y. and Matsuda, A.** (2006). Cavitation Erosion Resistance of Materials for Marine Propeller Application, *Materials Transactions*, *47*(4), 1227–1233.

[45] **Kinoshita, T.**, **Hino, T.**, **Yamaguchi, H. and Morita, M.** (2016). Effects of Hydrofoil Shape on Cloud Cavitation, *Journal of Fluids Engineering*, *138*(6), 061303.

[46] **McKeegan, W.**, **Hudson, D.**, **Stone, B. and Tao, L.** (2008). Cavitation Inception on Marine Propellers: A Review, *Applied Mechanics Reviews*, *61*(2), 020802.

[47] **Huse, E.** (1972). Propeller–hull vortex cavitation, *International Shipbuilding Progress*, *19*(212), 111–125.

[48] **Bosschers, J.** (2018). *Propeller Tip-Vortex Cavitation and its Broadband Noise*.

[49] **Tachmindji, A. and Morgan, W.** (1958). The design and estimated performance of a series of supercavitating propellers, *Proc. of 2nd Office of Naval Research Symposium on Naval Hydrodynamics*, pp.489–532.

[50] **Burrill, L. and Emerson, A.** (1963). Propeller cavitation: Further tests on 16in. propeller models in the King's College cavitation tunnel, *International Shipbuilding Progress*, *10*(104), 119–131.

[51] **Keller, A.e.a.** (1966). Pervane tasarımının bazı yönleri, *Schip en Werf*, *33*(24), 658–663.

[52] **Booker, J.M. and Ross, T.J.** (2011). An evolution of uncertainty assessment and quantification, *Scientia Iranica*, *18*(3), 669–676.

[53] **Rouvray, D.H.** (1996). *Fuzzy sets and fuzzy logic: Theory and applications: By GJ Klir and B. Yuan. Pp. 574. Prentice-Hall, 1995. ISBN 0 13 101171 5*.

[54] **Lacor, C.**, **Dinescu, C.**, **Hirsch, C. and Smirnov, S.** (2013). Implementation of intrusive polynomial chaos in CFD codes and application to 3D Navier-Stokes, *Uncertainty quantification in computational fluid dynamics*, 193–223.

[55] (2016). *Dakota Software Training, Uncertainty Quantification*, `https://dakota.sandia.gov/sites/default/files/training/DakotaTraining_UncertaintyQuantification.pdf`, accessed: 2023–01-21.

[56] **Smith, R.C.** (2013). *Uncertainty quantification: theory, implementation, and applications*, volume 12, Siam.

[57] **George-Williams, H.**, **Santhosh, T.V. and Patelli, E.** (2022). Simulation Methods for the Analysis of Complex Systems, Springer International Publishing, Cham, pp.95–113, `https://doi.org/10.1007/978-3-030-83640-5_7`.

[58] **Thoft-Christensen, P. and Baker, M.** (1982). STRUCTURAL RELIABILITY1, *Theory and its Applications*.

[59] **Der Kiureghian, A.** (1996). Structural reliability methods for seismic safety assessment: a review, *Engineering structures*, *18*(6), 412–424.

[60] **Zio, E.**, **Baraldi, P. and Patelli, E.** (2006). Assessment of the availability of an offshore installation by Monte Carlo simulation, *International Journal of Pressure Vessels and Piping*, *83*(4), 312–320.

[61] **Madsen, H.**, **Krenk, S. and Lind, N.** (2006). Methods of structural safety. Mineola, *NY: Dover Publications*.

[62] **Melchers, R.** (1989). Importance sampling in structural systems, *Structural safety*, *6*(1), 3–10.

[63] **Engelund, S. and Rackwitz, R.** (1993). A benchmark study on importance sampling techniques in structural reliability, *Structural safety*, *12*(4), 255–276.

[64] **Bucher, C.G.** (1988). Adaptive sampling—an iterative fast Monte Carlo procedure, *Structural safety*, *5*(2), 119–126.

[65] **Taheriyoun, M. and Moradinejad, S.** (2015). Reliability analysis of a wastewater treatment plant using fault tree analysis and Monte Carlo simulation, *Environmental monitoring and assessment*, *187*, 1–13.

[66] **Wang, C. and Qiu, Z.** (2014). An interval perturbation method for exterior acoustic field prediction with uncertain-but-bounded parameters, *Journal of Fluids and Structures*, *49*, 441–449.

[67] **Wang, Q. and Mu, M.** (2015). A new application of conditional nonlinear optimal perturbation approach to boundary condition uncertainty, *Journal of Geophysical Research: Oceans*, *120*(12), 7979–7996.

[68] **Fontanella, L. and Ippoliti, L.**, (2012). Karhunen–loéve expansion of temporal and spatio-temporal processes, Handbook of Statistics, volume 30, Elsevier, pp.497–520.

[69] **Xiu, D. and Tartakovsky, D.M.** (2006). Numerical methods for differential equations in random domains, *SIAM Journal on Scientific Computing*, *28*(3), 1167–1185.

[70] **Rifkin, R.M. and Lippert, R.A.** (2007). Notes on regularized least squares.

[71] **Crestaux, T.**, **Le Maıtre, O. and Martinez, J.M.** (2009). Polynomial chaos expansion for sensitivity analysis, *Reliability Engineering & System Safety*, *94*(7), 1161–1172.

[72] **Xiu, D.** (2010). *Numerical methods for stochastic computations: a spectral method approach*, Princeton university press.

[73] **Lee, S.H. and Chen, W.** (2009). A comparative study of uncertainty propagation methods for black-box-type problems, *Structural and multidisciplinary optimization*, *37*, 239–253.

[74] **Du, X.**, **Chen, W. and Wang, Y.** (2010). Most probable point-based methods, *Extreme Statistics in Nanoscale Memory Design*, 179–202.

[75] **Hasofer, A.M. and Lind, N.C.** (1974). Exact and invariant second-moment code format, *Journal of the Engineering Mechanics division*, *100*(1), 111–121.

[76] **Cai, G. and Elishakoff, I.** (1994). Refined second-order reliability analysis, *Structural Safety*, *14*(4), 267–276.

[77] **Evans, D.H.** (1972). An application of numerical integration techniques to statistical tolerancing, III—general distributions, *Technometrics*, *14*(1), 23–35.

[78] **Lee, S.H. and Kwak, B.M.** (2006). Response surface augmented moment method for efficient reliability analysis, *Structural safety*, *28*(3), 261–272.

[79] **Mohammadi, S. and Cremaschi, S.**, (2019). Efficiency of uncertainty propagation methods for estimating output moments, Computer Aided Chemical Engineering, volume 47, Elsevier, pp.487–492.

[80] **Rahman, S. and Xu, H.** (2004). A univariate dimension-reduction method for multi-dimensional integration in stochastic mechanics, *Probabilistic Engineering Mechanics*, *19*(4), 393–408.

[81] **Youn, B.**, **Xi, Z.**, **Wells, L. and Wang, P.** (2006). Enhanced dimension-reduction (edr) method for sensitivity-free uncertainty quantification, *11th AIAA/ISSMO multidisciplinary analysis and optimization conference*, p.6977.

[82] (2015). *Dakota Software Training, Surrogate Models*, `https://dakota.sandia.gov/sites/default/files/training/DakotaTraining_SurrogateModels.pdf`, accessed: 2023–01-22.

[83] **Santner, T.J.**, **Williams, B.J.**, **Notz, W.I. and Williams, B.J.** (2003). *The design and analysis of computer experiments*, volume 1, Springer.

[84] **Gutmann, H.M.** (2001). A radial basis function method for global optimization, *Journal of global optimization*, *19*(3), 201–227.

[85] **Antony, J.** (2014). *Design of experiments for engineers and scientists*, Elsevier.

[86] **Helton, J.C.** (1997). Uncertainty and sensitivity analysis in the presence of stochastic and subjective uncertainty, *journal of statistical computation and simulation*, *57*(1-4), 3–76.

[87] **Robinson, D. and Atcitty, C.** (1999). Comparison of quasi-and pseudo-Monte Carlo sampling for reliability and uncertainty analysis, *40th Structures, Structural Dynamics, and Materials Conference and Exhibit*, p.1589.

[88] **Metropolis, N. and Ulam, S.** (1949). The monte carlo method, *Journal of the American statistical association*, *44*(247), 335–341.

[89] **McKay, M.D.**, **Beckman, R.J. and Conover, W.J.** (2000). A comparison of three methods for selecting values of input variables in the analysis of output from a computer code, *Technometrics*, *42*(1), 55–61.

[90] **Saliby, E.** (1990). Descriptive sampling: a better approach to Monte Carlo simulation, *Journal of the Operational Research Society*, *41*(12), 1133–1142.

[91] **Viana, F.A.** (2016). A tutorial on Latin hypercube design of experiments, *Quality and reliability engineering international*, *32*(5), 1975–1985.

[92] **Hammersley, J.M.** (1960). Monte Carlo methods for solving multivariable problems, *Annals of the New York Academy of Sciences*, *86*(3), 844–874.

[93] **Kalagnanam, J.R. and Diwekar, U.M.** (1997). An efficient sampling technique for off-line quality control, *Technometrics*, *39*(3), 308–319.

[94] **Sobester, A.**, **Forrester, A. and Keane, A.** (2008). *Engineering design via surrogate modelling: a practical guide*, John Wiley & Sons.

[95] **Torre, E.**, **Marelli, S.**, **Embrechts, P. and Sudret, B.** (2019). A general framework for data-driven uncertainty quantification under complex input dependencies using vine copulas, *Probabilistic Engineering Mechanics*, *55*, 1–16.

[96] **Najm, H.N.** (2009). Uncertainty quantification and polynomial chaos techniques in computational fluid dynamics, *Annual review of fluid mechanics*, *41*, 35–52.

[97] **Dwight, R.P.**, **Witteveen, J.A. and Bijl, H.** (2013). *Adaptive uncertainty quantification for computational fluid dynamics*, Springer.

[98] **Simpson, T.**, **Toropov, V.**, **Balabanov, V. and Viana, F.** (2008). Design and analysis of computer experiments in multidisciplinary design optimization: a review of how far we have come-or not, *12th AIAA/ISSMO multidisciplinary analysis and optimization conference*, p.5802.

[99] **Zhao, Y.**, **Lu, W. and Xiao, C.** (2016). A Kriging surrogate model coupled in simulation–optimization approach for identifying release history of groundwater sources, *Journal of Contaminant Hydrology*, *185*, 51–60.

[100] **Granados-Ortiz, F.J.**, **Arroyo, C.P.**, **Puigt, G.**, **Lai, C.H. and Airiau, C.** (2019). On the influence of uncertainty in computational simulations of a high-speed jet flow from an aircraft exhaust, *Computers & Fluids*, *180*, 139–158.

[101] **Friedman, J.H.** (1991). Multivariate adaptive regression splines, *The annals of statistics*, *19*(1), 1–67.

[102] **Jekabsons, G.** (2010). VariReg: a software tool for regression modelling using various modeling methods, *Riga Technical University*.

[103] **Kleinbaum, D.G.**, **Kupper, L.L.**, **Nizam, A. and Rosenberg, E.S.** (2013). *Applied regression analysis and other multivariable methods*, Cengage Learning.

[104] **Zhang, W.**, **Goh, A.T. and Zhang, Y.** (2016). Multivariate adaptive regression splines application for multivariate geotechnical problems with big data, *Geotechnical and Geological Engineering*, *34*, 193–204.

[105] **Won, K.S.**, **Ray, T. and Tai, K.** (2003). A framework for optimization using approximate functions, *The 2003 Congress on Evolutionary Computation, 2003. CEC'03.*, volume 3, IEEE, pp.1520–1527.

[106] **Won, K.S. and Ray, T.** (2005). A framework for design optimization using surrogates, *Engineering optimization*, *37*(7), 685–703.

[107] **Singh, R.M.**, **Datta, B. and Jain, A.** (2004). Identification of unknown groundwater pollution sources using artificial neural networks, *Journal of water resources planning and management*, *130*(6), 506–514.

[108] **Lancaster, P. and Salkauskas, K.** (1986). An introduction: curve and surface fitting, *Unpublished, Division of Applied Mathematics, University of Calgary*, *114*.

[109] **Breitkopf, P.**, **Rassineux, A. and Villon, P.** (2002). An introduction to moving least squares meshfree methods, *Revue européenne des éléments finis*, *11*(7-8), 825–867.

[110] **Roos, D.**, **Most, T.**, **Unger, J. and Will, J.** (2007). Advanced surrogate models within the robustness evaluation, *Proc. Weimarer Optimierungs-und Stochastiktage*, *4*, 29–30.

[111] **Peherstorfer, B.**, **Willcox, K. and Gunzburger, M.** (2018). Survey of multi-fidelity methods in uncertainty propagation, inference, and optimization, *Siam Review*, *60*(3), 550–591.

[112] **Zhang, J.**, **Chowdhury, S. and Messac, A.** (2012). An adaptive hybrid surrogate model, *Structural and Multidisciplinary Optimization*, *46*, 223–238.

[113] **Shimoyama, K. and Inoue, A.** (2016). Uncertainty quantification by the nonintrusive polynomial chaos expansion with an adjustment strategy, *AIAA journal*, *54*(10), 3107–3116.

[114] **Moustapha, M. and Sudret, B.** (2019). A two-stage surrogate modelling approach for the approximation of models with non-smooth outputs.

[115] **Sedwick, R. and Schweighart, S.** (2001). Development and analysis of a high fidelity linearized J (2) model for satellite formation flying, *AIAA space 2001 Conference and exposition*, p.4744.

[116] **Sakata, S.i.** (2014). Adaptive strategy for stochastic homogenization and multiscale stochastic stress analysis, *Multiscale Modeling and Uncertainty Quantification of Materials and Structures: Proceedings of the IUTAM Symposium held at Santorini, Greece, September 9-11, 2013.*, Springer, pp.51–66.

[117] **Lin, M.H.**, **Carlsson, J.G.**, **Ge, D.**, **Shi, J. and Tsai, J.F.** (2013). A review of piecewise linearization methods, *Mathematical problems in Engineering*, *2013*.

[118] **Zhang, X.Y.**, **Trame, M.N.**, **Lesko, L.J. and Schmidt, S.** (2015). Sobol sensitivity analysis: a tool to guide the development and evaluation of systems pharmacology models, *CPT: pharmacometrics & systems pharmacology*, *4*(2), 69–79.

[119] **Sobol, I.M.** (1993). Sensitivity analysis for non-linear mathematical models, *Math. Modeling Comput. Exp.*, *1*, 407–414.

[120] **Saltelli, A.**, **Tarantola, S. and Chan, K.S.** (1999). A quantitative model-independent method for global sensitivity analysis of model output, *Technometrics*, *41*(1), 39–56.

[121] **Homma, T. and Saltelli, A.** (1996). Importance measures in global sensitivity analysis of nonlinear models, *Reliability Engineering & System Safety*, *52*(1), 1–17.

[122] **Sobol', I.M.** (2005). Global sensitivity indices for the investigation of nonlinear mathematical models, *Matematicheskoe modelirovanie*, *17*(9), 43–52.

[123] **Saltelli, A.**, **Annoni, P.**, **Azzini, I.**, **Campolongo, F.**, **Ratto, M. and Tarantola, S.** (2010). Variance based sensitivity analysis of model output. Design and estimator for the total sensitivity index, *Computer physics communications*, *181*(2), 259–270.

[124] **Weirs, V.G.**, **Kamm, J.R.**, **Swiler, L.P.**, **Tarantola, S.**, **Ratto, M.**, **Adams, B.M.**, **Rider, W.J. and Eldred, M.S.** (2012). Sensitivity analysis techniques applied to a system of hyperbolic conservation laws, *Reliability Engineering & System Safety*, *107*, 157–170.

[125] **Herman, J. and Usher, W.** (2017). SALib: An open-source Python library for sensitivity analysis, *Journal of Open Source Software*, *2*(9), 97.

[126] **AWvd, V.** (1998). *Asymptotic Statistics. Cambridge Series in Statistical and Probabilistic Mathematics*.

[127] **Eça, L. and Hoekstra, M.** (2014). A procedure for the estimation of the numerical uncertainty of CFD calculations based on grid refinement studies, *Journal of computational physics*, *262*, 104–130.

[128] **Land, N.S.** (1943). Characteristics of an NACA 66, S-209 section hydrofoil at several depths, **Technical Report**.

[129] **Ducoin, A.**, **Huang, B. and Young, Y.L.** (2012). Numerical modeling of unsteady cavitating flows around a stationary hydrofoil, *International Journal of Rotating Machinery*, *2012*.

[130] **Hidalgo, V.**, **Luo, X.**, **Escaler, X.**, **Ji, J. and Aguinaga, A.** (2014). Numerical investigation of unsteady cavitation around a NACA 66 hydrofoil using OpenFOAM, *IOP Conference Series: Earth and Environmental Science*, volume 22, IOP Publishing, p.052013.

[131] **Amano, R.S.**, **Qandil, M.**, **Elgammal, T.**, **Abbas, A. and Abdelhadi, A.** (2019). Predicting the Cavitation Phenomena Over the Hydrofoil: CFD Validation, *AIAA Scitech 2019 Forum*, p.0783.

[132] **Shen, Y.T. and Eppler, R.** (1981). Wing sections for hydrofoils—part 2: Nonsymmetrical profiles, *Journal of ship research*, *25*(03), 191–200.

[133] **Francis, T. and Katz, J.** (1988). Observations on the development of a tip vortex on a rectangular hydrofoil.

[134] **Dimotakis, P.**, **Gaebler, H.**, **Hamaguchi, H.**, **Lang, D. and Shen, Y.** (1987). Two-dimensional NACA 66 (MOD) hydrofoil High Speed Water Tunnel tests.

[135] **Vaz, G.**, **Toxopeus, S. and Holmes, S.** (2010). Calculation of manoeuvring forces on submarines using two viscous-flow solvers, *International Conference on Offshore Mechanics and Arctic Engineering*, volume49149, pp.621–633.

[136] **Schnerr, G.H. and Sauer, J.** (2001). Physical and Numerical Modeling of Unsteady Cavitation Dynamics, *ICMF-2001, 4th International Conference on Multiphase Flow*, event-place: New Orleans, Louisiana, United States.

[137] **Leroux, J.B.**, **Coutier-Delgosha, O. and Astolfi, J.A.** (2005). A joint experimental and numerical study of mechanisms associated to instability of partial cavitation on two-dimensional hydrofoil, *Physics of fluids*, *17*(5), 052101.

[138] **Brouwer, J.**, **Tukker, J.**, **Van Rijsbergen, M.** *et al.* (2013). Uncertainty analysis of finite length measurement signals, *The 3rd International Conference on Advanced Model Measurement Technology for the EU Maritime Industry (AMT'13), Gdansk, Poland*, pp.260–274.

[139] **Brouwer, J.**, **Tukker, J. and van Rijsbergen, M.** (2015). Uncertainty Analysis and Stationarity Test of Finite Length Time Series Signals.

[140] **Brouwer, J.**, **Tukker, J.**, **Klinkenberg, Y. and van Rijsbergen, M.** (2019). Random uncertainty of statistical moments in testing: Mean, *Ocean Engineering*, *182*, 563–576.

[141] **Lemaire, S. and Klapwijk, M.** (2021). *pyTST*, `https://doi.org/10.5281/zenodo.4428158`.

CURRICULUM VITAE

Name SURNAME: Erdinç KARA

EDUCATION:

- **B.Sc.:** 2020, Istanbul Technical University, Shipbuilding and Ocean Engineering Faculty, Shipbuilding and Ocean Engineering

PROFESSIONAL EXPERIENCE AND REWARDS:

- 2022 Maritime Research Institute Netherlands - Scholar
- 2022 Istanbul Technical University - Research Assistant
- 2021 NAVTEK Naval Technologies Inc. - R&D Engineer
- 2020 Atlas Shipyard - Planning / Outfitting Engineer